DOT/FAA/TC-20/8

Federal Aviation Administration
William J. Hughes Technical Center
Aviation Research Division
Atlantic City International Airport
New Jersey 08405

Multi-Functional Cell Packaging for Prevention of Failure Propagation and Runaway in Lithium-Ion Batteries for Aviation Applications

April 2020

Final Report

U.S. Department of Transportation
Federal Aviation Administration

NOTICE

Technical Report Documentation Page

1. Report No.	2. Government Accession No.	3. Recipient's Catalog No.
DOT/FAA/TC-20/8		

4. Title and Subtitle	5. Report Date
Multi-Functional Cell Packaging for Prevention of Failure Propagation and Runaway in Lithium-Ion Batteries for Aviation Applications	April 2020
	6. Performing Organization Code

7. Author(s)	8. Performing Organization Report No.
Avijit Bhunia, Kyle Gould, Rick Sickenberger, Janak Rajpara, and Joshua Lamb	

9. Performing Organization Name and Address	10. Work Unit No. (TRAIS)
Teledyne Scientific Company 1049 Camino Dos Rios, Thousand Oaks, CA, 91360	
	11. Contract or Grant No. DTFACT-16-C-00044

12. Sponsoring Agency Name and Address	13. Type of Report and Period Covered
Federal Aviation Administration William J. Hughes Technical Center Aviation Research Division Atlantic City International Airport New Jersey 08405	Final Report
	14. Sponsoring Agency Code ANM-111

15. Supplementary Notes

The Federal Aviation Administration William J. Hughes Technical Center Aviation Research Division COR was Michael Walz.

16. Abstract

Engine starter batteries for aircraft applications need to deliver high instantaneous power. Current Lead acid and nickel cadmium technologies fulfil this requirement. Li-ion batteries, on the other hand, can deliver this power at significantly reduced battery size and weight. However, current Li-ion batteries suffer from two key challenges: (a) Safety, i.e. thermal runaway of Li-ion batteries leading to catastrophic failures of installation platforms, and (b) Limited cycle life due to cell temperature rise at high discharge/ charge rates. In this program, Teledyne and its team members investigated a Li-ion cell packaging technology that simultaneously addresses both. The technology was utilized to develop prototypes of 26 V, 20 Ah batteries, using pouch cells of highly volatile lithium cobalt oxide chemistry. The effectiveness of the technology in preventing catastrophic thermal runaway was tested under Battery Management System disabled condition for various abuse cases. Tests were conducted from cell-level, to module-level, and finally to the full battery-level. Results show no cell-to-cell failure propagation at the module-level. At the full battery-level, with more than one trigger cells, failure propagation and catastrophic thermal runaway could be prevented as long as the effluents of the failed cells were vented properly. The packaging technology resulted in a small rise in cell temperature during deep discharge of the battery, which enables improved cycle life. The 26 V, 20 Ah Li-ion battery built as a demonstration platform of the packaging technology, is of the same size as the current lead acid battery, but 2.3X lighter.

17. Key Words	18. Distribution Statement
Li-ion batteries, Safety, Thermal runaway prevention, Thermal management	This document is available to the U.S. public through the National Technical Information Service (NTIS), Springfield, Virginia 22161. This document is also available from the Federal Aviation Administration William J. Hughes Technical Center at actlibrary.tc.faa.gov.

19. Security Classif. (of this report)	20. Security Classif. (of this page)	21. No. of Pages	22. Price
Unclassified	Unclassified	51	$419,022

ACKNOWLEDGEMENTS

The authors gratefully acknowledge the financial support from FAA; the technical discussions, feedback, and input from the Program Manager Mr. Michael Walz; and the technical/ management help in program execution from a number of people at Teledyne Technology, namely: Bobby Brar, Alex Diaz, Mark Gardner, Alex Moffatt, Charles Neft, and Chanh Nguyen.

TABLE OF CONTENTS

LIST OF FIGURES

LIST OF TABLES

LIST OF ACRONYMS

AFRL	Air Force Research Lab
BMS	Battery Management System
FEA	Finite element analysis
FoS	Factor of Safety
GUI	Graphical user interface
HESM	High-energy storage module
LCO	Lithium cobalt oxide
LFP	Lithium iron phosphate
MBB	Modular building block
RTCA	Radio Technical Commission for Aeronautics
SNL	Sandia National Laboratories

EXECUTIVE SUMMARY

The goal of this FAA program was to explore a packaging technology for developing safe aviation batteries with Li-ion chemistry. Teledyne Scientific Company and its team members, Teledyne Energy Systems, Inc.; Teledyne Battery Products (TBP); and Sandia National Laboratories (SNL), investigated the suitability of the technology to prevent the cascading effect of cell-to-cell failure propagation inside a battery and the resulting catastrophic thermal runaway. As a demonstration platform, the Teledyne team chose to build a 26 V, 20 Ah Li-ion battery. The rating and physical size of the battery were chosen with a potential future product in mind (beyond the scope of this program), that is, to replace TBP's FAA-certified 24 V, 20 Ah Robinson R-66 aircraft lead acid battery (cat. no. 7246-20) with a Li-ion version.

The passive (no moving parts) packaging technology is multi-functional, simultaneously addressing the safety and thermal management (cycle life) aspects of Li-ion batteries. Each cell of the battery is wrapped with the packaging material that acts as a cell level thermal management system. In the event of a local cell failure, heat generated from the runaway cell is absorbed by the packaging material in direct contact with the heat dissipating cell, lowering its temperature rise, preventing heat dump to the neighboring cell, and thus the cascading effect. The same mechanism does the thermal management under normal operating conditions, such as engine starts or cruise. The packaging concept is external to the cell, and therefore applicable to all cell chemistries and form factors. Teledyne first developed and demonstrated the concept under an internally funded R&D program. The technology was further developed and demonstrated at cell array level under an Air Force Research Lab (AFRL)-funded program (08/2014 to 03/2016). Subsequently, under continued AFRL funding (07/2016 – 03/2018), Teledyne incorporated this technology to design and build a 78 V, 5 Ah, 12 kW high-power density battery for instantaneous power delivery to high-energy laser. The 12 kW battery was built with three fully self-contained 26V, 5 Ah modular building blocks (MBBs), externally connected in series and controlled by a master battery management system (BMS). Each MBB contained seven power dense, highly volatile lithium cobalt oxide (LCO) chemistry cells rated at 3.7 V and 5 Ah and a fully incorporated slave BMS. There was a time overlap between the AFRL 12 kW battery development program and this FAA-funded program, resulting in significant leverage from one another. For example: based on the initial success of the AFRL program (in prevention of cell-to-cell failure propagation in the MBB), there was a change in cell chemistry choice in the current FAA program. We built the 26 V, 20 Ah battery using highly volatile LCO chemistry, as opposed to the original program plan of lithium iron phosphate chemistry. LCO provided higher-power density and a better use case to prove the efficacy of the technology.

As a demonstration platform, we developed, prototyped, and tested 26 V, 20 Ah batteries. Each battery was built with 28 pouch cells of LCO chemistry in a 7S4P configuration, with the cells wrapped in the packaging technology. We also built a BMS with over/under voltage, over current, short circuit, and over/under temperature protection. As a functional test, the batteries were operated under helicopter starter load profiles, delivering instantaneous current ratings of 756 amps (for 0.3 s, commonly termed as I_{pp} in avionics starter battery) and 403 amps (for 15 s, commonly termed as I_{pr}). We also tested the fast charging capability of the battery (at 4C rate or 80 amps). The cell case temperature rise was < 10°C for all high-current discharge tests, which allows the battery to perform multiple aircraft engine starts without risk of thermal damage and reduced cycle life.

Most of the work in this program focused on investigating the safety angle. These lithium batteries were subjected to mechanical, thermal, and electrical abuse conditions at the test facility of team member SNL. The abuse tests were carried out first at single cell-level (3.7 V, 5 Ah), then at module-level (3.7 V, 20 Ah in 1S4P configuration), then at multi-module-level (11.1 V, 20 Ah in 3S4P configuration), and finally at full battery level (25.9 V, 20 Ah in 7S4P configuration). The packaging technology is designed to prevent cell-to-cell failure propagation. Therefore, at the single cell-level, there was no prevention. Substantial prevention of cell-to-cell failure propagation was demonstrated at module and multi-module levels. At the full battery level, failure propagation tests were carried out with single and multiple cell failure (two trigger cells) at the worst failure configuration. The results show no cell-to-cell failure propagation as long as the effluents of the failed cells are vented out, preventing heat propagation through the ejecta. The full battery-level tests underscored the importance of venting in addition to the thermal dump to the neighboring cells.

After a successful closure of the FAA-funded program, Teledyne is exploring opportunities to mature the technology further and raise its manufacturing readiness level. Future efforts need to focus on: (1) further investigating battery venting design to increase likelihood of failure-propagation prevention for multi-cell failures; (2) establishing long-term reliability and ruggedization for airborne applications; and, finally, (3) FAA qualification testing, including DO-311A tests.

1. INTRODUCTION

1.1 SAFETY ISSUES OF LITHIUM-ION BATTERY SYSTEMS

Energy storage based on Lithium-ion chemistry offers significant size and weight benefits over traditional lead acid or nickel cadmium batteries. In spite of its well-proven power and energy density benefits, adoption of Li-ion battery has been slow because of safety concerns, fueled by several “high profile” catastrophic failures. The catastrophic event of a Li-ion battery usually starts with a single cell failure. The failure can be triggered by several mechanisms, such as an internal short, mechanical damage, electrical overcharge, or over temperature (external heating of a cell), all leading to heating of the failed cell. If the resulting cell temperature rise exceeds a certain threshold, several other exothermic reactions are initiated inside the cell, resulting in more heat release and further temperature rise. A local cell failure, once initiated, cannot be controlled. However, a much bigger problem arises when the released energy from the failed cell is dumped into its neighboring cells. It can initiate a similar chain reaction in the neighboring cells, triggering another failure, and so on, until the entire battery is on fire. Figure 1 shows a battery with catastrophic failure induced by this chain reaction of cell-to-cell failure propagation. Among the various Li-ion chemistries, the higher power and energy density chemistries are usually more susceptible and have more damaging effects. Flammable electrolytes and oxide-based cathodes, such as lithium cobalt oxide (LCO) or lithium manganese oxide are some examples, which have the propensity of decomposing auto-catalytically with a highly exothermic reaction.

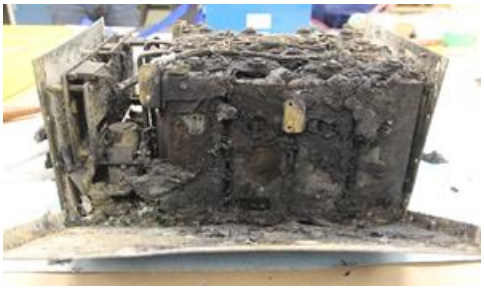

Figure 1. An example of a catastrophic failure of a large lithium-ion battery, initiated by a thermal runaway of a single cell and subsequent chain reaction of failure propagation

A variety of safety features, such as shunts, pressure release valves, and battery management systems (BMSs), are typically implemented. These preventive measures are necessary but not sufficient, as they cannot avert the domino effect. Physically stopping the cascading effect is vital for the runaway prevention and mitigation of battery failure. The “Minimum Operational Performance Standards for Rechargeable Lithium Batteries and Battery Systems”, recently completed by a special committee (SC-225) of Radio Technical Commission for Aeronautics (RTCA) DO-311A, indicates that mitigation of cell and battery failure will be a critical qualification requirement for li-ion batteries in aviation platforms.

1.2 STATE-OF-THE-ART METHODS AND THEIR LIMITATIONS

In most commercially available small (< 60 Ah capacity) Li-ion batteries, cells are packed tightly together in a specific series-parallel configuration to achieve a desired voltage and capacity. The cells rely solely on buoyancy-driven natural circulation of air inside and outside the battery box

for cooling (figure 2a). The thermal management is not effective, leading to heat buildup, rapid cell degradation, and dramatic reduction in cycle life at high discharge/charge rates. To minimize the thermal build up in normal operating conditions and the issue of cycle life reduction, Li-ion battery manufacturers typically lower cell discharge rates by placing more cells in parallel than necessary. Furthermore, tightly packed cells have a high risk of catastrophic failure due to energy from a failed cell being dumped to neighboring cells. To address the safety concerns, cells are physically separated from each other or placed in an insulative environment of solid-to-liquid phase change materials (figure 2b). As a result, much of the benefit of lithium chemistry (higher power and energy density, compared to conventional battery chemistries) is lost. These passive solutions do not effectively solve the issues of high power/energy density desired for airborne applications. Electric vehicle batteries are often actively cooled by pumping liquid in between cells (figure 2c). The thermal management and safety concerns of Li-ion batteries are addressed. However, additional system complexity may lead to higher size and weight penalties, and cost of ownership. There is also the potential for failure introducing new failure mechanisms, such as internal short by coolant-borne particles involving coolant leak.

(a) (b) (c)

Figure 2. State-of-the-art of thermal management and safety technologies in Li-ion batteries: (a) tightly packed cells with natural convection air circulation cooling; (b) graphite casing with solid-to-liquid phase change material to absorb heat from a failed cell to prevent thermal runaway; and (c) active liquid cooling channels in between each cell

2. TECHNOLOGY OVERVIEW AND OBJECTIVE OF PROGRAM

2.1 CONCEPT OF OPERATION OF THE PACKAGING TECHNOLOGY

Figure 3 shows the concept of operation of Teledyne's cell-packaging technology. The packaging material is wrapped around each individual cell, allowing for heat released by the cell to be dissipated to the packaging technology through direct contact. In case of a cell failure, heat generated from the runway cell is absorbed by the packaging material, lowering its temperature rise and preventing heat dump to the neighboring cell. Under normal operation, the heat absorbed at the cell wall by the packaging technology is transported to the battery box wall, from where it is dissipated to the ambient. The heat transport system is a passive, closed-loop system that continuously moves heat from the cell wall to the battery box wall.

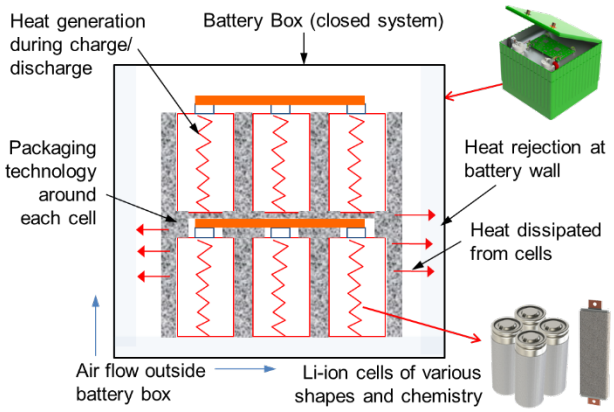

Figure 3. Operational concept of Teledyne's cell-packaging technology

Salient features of the technology are:

- *Multi-functionality of the cell packaging:* A single unique solution for both thermal management and failure containment. Under normal operating conditions, it acts as a cell thermal management system. Under fault conditions, the self-adaptive mechanism of the technology ensures that the packaging materials on surrounding cells come to the rescue of a runaway cell. As a result, temperature rise of the failed cell is controlled, reducing the exothermic reaction and heat dump to neighboring cells.
- *Passive, self-contained, thermal management system*: Heat absorption at the cell wall and heat rejection at the module wall establish a highly efficient, closed loop, passive thermal transport between the cell and module walls. Therefore, the thermal problem is shifted from the cell level to the battery box outer-wall level through a very low thermal resistance path.
- *System complexity, cost, and safety*: Being a completely self-contained system without direct contact with the external environment, it significantly reduces the thermal management system complexity and cost, and avoids any chance of accidental coolant-borne short.
- *A high degree of temperature uniformity among cells in a large battery* enabled by the self-regulating nature of the technology.
- *Agnostic to cell chemistry and form factor*: Being an external packaging technology, it can be used for any chemistry and form factor (cylindrical, pouch, prismatic). The packaging structure can be designed to fit a specific form factor.

2.2 STATUS OF THE PACKAGING TECHNOLOGY PRIOR TO THIS PROGRAM

Teledyne first developed and demonstrated the packaging technology concept under an internally funded research and development program. To prove that the cell surface temperature can be maintained at a reasonable level (typically < 5°C temperature rise above ambient) at discharge rates up to 8C, 26650 cylindrical cells of lithium iron phosphate (LFP) chemistry were used. The technology was further developed and demonstrated at the cell array level under the Air Force Research Lab (AFRL)-funded High-energy storage module (HESM) program (08/2014 – 03/2016). An array of 4 to 7 of 26650 LFP cells was used in this program to demonstrate the efficacy of the packaging solution in: (a) maintaining moderate cell temperature at high

discharge rate (up to 21C rate deep discharge) and (b) preventing failure propagation from a failed cell to its neighboring cell. At 21C rate deep discharge, cell temperature rise (above ambient) was capped at ~10°C. Failure of the LFP cell array was triggered by a mechanical nail penetration, and prevention of cell-to-cell failure propagation was demonstrated. Successful data of the HESM program encouraged us to send two subsequent proposals, written almost concurrently, one to FAA (the current program) and another to AFRL to develop a high power density battery for high energy laser application. A few months prior to starting the current FAA-funded program, the AFRL continuation program was awarded for designing and building a very high power density, 78 V/ 5 Ah/ 12 kW battery, incorporating the packaging technology (07/2016 – 03/2018). The 12 kW density battery was designed for instantaneous power delivery to high-energy lasers and was built with three fully self-contained 26V, 5 Ah modular building blocks (MBBs), externally connected in series and controlled by a master BMS. Each MBB contained seven power-dense, highly volatile LCO chemistry cells, rated at 3.7 V and 5 Ah and a fully incorporated slave BMS.

There was a time overlap between the AFRL 12 kW battery-development program and this FAA-funded program, resulting in significant leverage from one another. For example: based on the initial success of the AFRL program (in prevention of cell-to-cell failure propagation in the MBB), there was a change in cell chemistry choice in the current FAA program. In the original proposal (to FAA), the building of a demonstrator battery using 26650 LFP cells was planned. At the time of the kickoff meeting of this FAA-funded program (March 2017), Teledyne and the FAA mutually agreed to switch to a more volatile LCO chemistry. Therefore, the 26 V, 20 Ah demonstrator battery was built using LCO pouch cells. LCO provided higher power density and a better use case to prove the efficacy of the packaging technology, particularly the cell-to-cell failure propagation aspect of it.

2.3 OBJECTIVE OF THE CURRENT PROGRAM

The main objective of the current program was to investigate the effectiveness of the packaging technology in prevention of cell-to-cell failure propagation and addressing the safety concern of lithium-ion batteries in airborne platforms. The packaging concept is external to the cell and therefore applicable to all cell chemistries and form factors (figure 4).

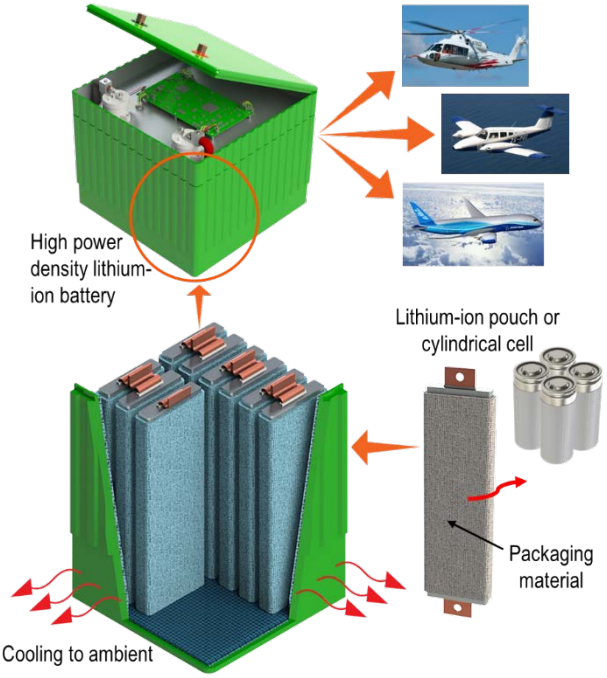

Figure 4. Safe, high-power-density lithium-ion battery for avionics applications, incorporating Teledyne's multi-functional cell packaging technology, simultaneously addressing safety and thermal management of Li-ion batteries

As a demonstration platform, prototypes of 26 V, 20 Ah Li-ion batteries equipped with the passive, self-adaptive, fully enclosed, cell-packaging technology were built. At the beginning of the project, some failure propagation data from the 26 V, 5 Ah MBB in the AFRL-funded 12 kW battery development program had accumulated. With the initial indication of prevention of cell-to-cell propagation at 5 Ah level, the objective of the current FAA-funded program was to investigate the scalability to a higher capacity (20 Ah) cell block or module, then to multiple modules, and finally to the full-scale 26 V, 20 Ah battery.

3. DEMONSTRATION PLATFORM (26 V, 20 AH BATTERY) – DESIGN, FABRICATION, AND TESTING

3.1 CHOICE OF CELL

The initial proposed plan was to use 3.3 V, 2.85 Ah LFP chemistry 26650 (26 mm diameter and 65 mm tall) cylindrical power cells from K2 Energy Systems. These cells have a specific energy of 112 Wh/kg. As discussed in section 2.2, at the program kickoff meeting (March 2017), the Teledyne and the FAA Program Manager collectively decided to switch to Kokam SLPB11543140H5 power cells (3.7 V, 5 Ah in pouch configuration) with LCO chemistry. Specifications of the cell are shown in table 1. The LCO cell cathode is an extremely power dense lithium-ion chemistry capable of delivering up to 150 amp continuous and 250 amp pulsed current. However, being an oxide-based chemistry, LCO has the propensity of decomposing autocatalytically; that is, the cathode decomposition generates oxygen that reacts exothermically with organics in the cell (e.g., electrolyte, graphite), further increasing the temperature and

promoting further decomposition of the cathode. That makes the LCO chemistry cells highly volatile with a strong tendency to go into thermal runaway. The broad rationale behind the switch in choice of cell were threefold:

1. The inherent volatility of the LCO chemistry cell (more than the LFP chemistry) made it a more appealing candidate for this proof-of-concept study.
2. The 5 Ah LCO cell has ~30% higher energy density (140 Wh/kg compared to 112 Wh/kg for the 26650 LFP cell), so if the cells went into a runaway mode, it had more energy content (a better platform for proof-of-concept demo of the technology).
3. The 5 Ah capacity ensured that the energy content of a single failed cell was manageable by the packaging technology.

Table 1. Kokam cell specifications

Kokam SLPB11543140H5	
Rated Capacity	5.0 Ah
Nominal Voltage	3.7 V
End of Discharge	3.0 V
AC Impedance	< 3.0 mΩ
Max. Charge Voltage	4.2 V
Max. Conti. Charge Current	10.0 A (2C)
Max. Conti. Discharge Current	150.0 A (30C)
Operating Temp. Range	Charge: 0 – 45 °C
	Discharge: -20 – 55 °C
Weight	132 g
Cell Dimensions	L: 142.5 mm
	W: 43.5 mm
	T: 11.7 mm

Figure 5 shows the cell vendor provided cell discharge curves at various discharge rates. Because the intended application for the 26 V, 20 Ah battery was a helicopter starter battery, an instantaneous current rating (for 0.3 s and 15 s) of the cell was generated. A constant voltage discharge of a single cell at 3 V (LCO chemistry suggested cut-off voltage) was performed for 15 s. The results are shown in figure 6. The testing was limited to 240 amps due to equipment limitations. It is evident that the cell is capable of delivering more than 240 A peak discharge rate for several seconds and ≥ 150 A for at least 15 seconds. Therefore, with 4 cells in parallel, the 20 Ah capacity Li-ion battery would be theoretically capable of delivering an I_{pp} (starter battery current delivered over 0.3 s) and I_{pr} (starter battery current delivered over 15 s) of 1000 A and 600 A respectively.

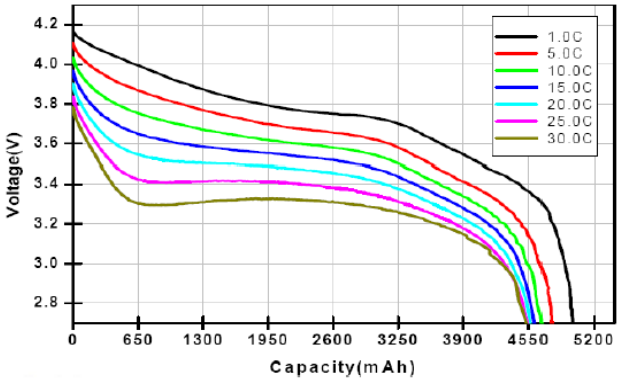

Figure 5. Discharge characteristics of the Kokam SLPB11543140H5 LCO cell

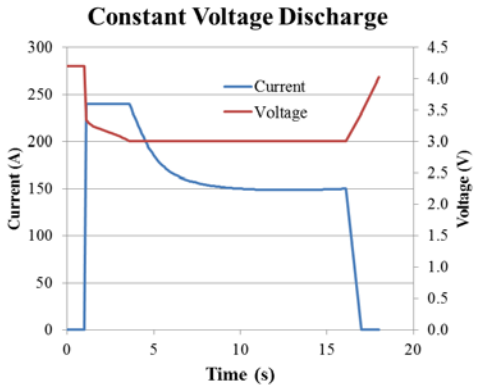

Figure 6. Constant voltage (3 V) discharge of a single Kokam LCO pouch cell for 15 s; current limited to 240 A because of equipment limitations

3.2 SYSTEM DEFINITION

The battery system for this program was a 26 V, 20 Ah Li-ion battery, chosen as a demonstration platform for the packaging technology. The rating and physical size of the battery were chosen with a potential future product in mind (beyond the scope of this program): that is, to replace team member Teledyne Battery Products (TBP)'s FAA-certified 24 V, 20 Ah Robinson R-66 aircraft lead acid battery (catalogue number 7246-20) with a Li-ion version. Therefore, the 7246-20 battery (20 kg, 8.1 L) shown in figure 7 served as the baseline system, against which an equivalent Li-ion battery system would be compared. To match the 20 Ah capacity of the TBP's current VRLA battery, four 5 Ah LCO cells were used in parallel. Then, to reach the desired nominal voltage, seven cells were used in series. Therefore, the full-scale battery system had a 7S4P configuration of cells.

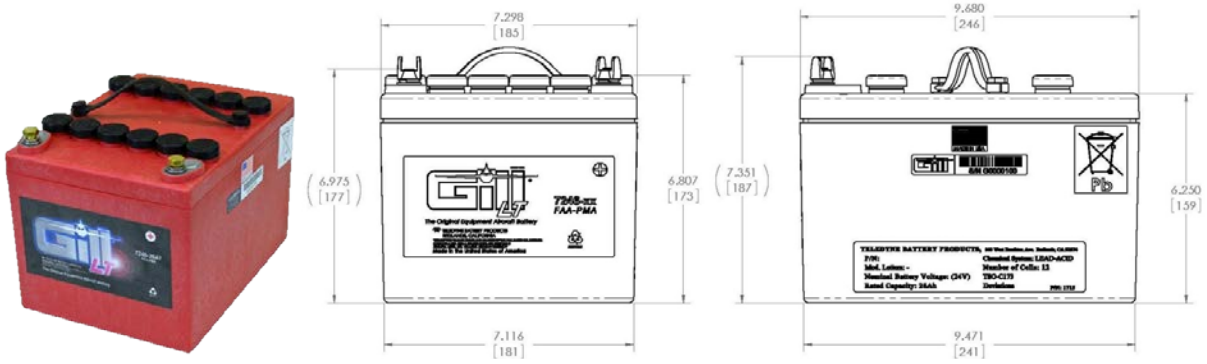

Figure 7. Teledyne battery products (TBP) valve-regulated lead acid (VRLA) battery 7246-20, rated at 24 V, 20 Ah, currently undergoing TSO certification

Table 2 presents the specifications of the 26 V, 20 Ah demonstrator Li-ion battery system and its comparison with baseline the 7246-20 VRLA battery.

Table 2. Specifications for Li-ion battery with incorporating the packaging technology, and its comparison with the current 7246-20 valve regulated lead acid (VRLA) battery.

	Li-ion Battery with Teledyne packaging technology	Teledyne's current valve regulated lead acid (VRLA) battery (7246-20)
Capacity	20 Ah	20 Ah
Output Voltage	25.9 VDC nominal	24 VDC nominal
I_{pp} @ 23 °C	1000 A*	1250 A
I_{pr} @ 23 °C	600 A*	860 A
Charge Voltage	29.4 VDC	28.5 VDC
Charge Current	80 A (max.)	300 A (max.)
Size	9.68" x 7.30" x 6.98" (8.1 L)	9.68" x 7.30" x 6.98" (8.1 L)
Weight	19.2 lbs. (8.7 kg)	44.0 lbs. (20.0 kg)
Specific Energy	64.0 Wh/L	59.3 Wh/L
Energy Density	59.5 Wh/kg	24 Wh/kg
Operating Temp.	-20 – 55 °C	-20 – 50 °C
Cell configuration	7S4P	12S1P
Protection	Over/under voltage, over current, short circuit, and over/under temperature protection through BMS	n/a
Safety	No cell-to-cell failure propagation, thermal runaway	n/a
External Cooling	Uncooled	n/a
Case	Aluminum	Polypropylene

* Performance during constant voltage 21 V 15 s discharge.

One notable point of departure between the Li-ion and the VRLA batteries is the instantaneous discharge current performance. The VRLA battery is rated for I_{pp} (current over 0.3 s) and I_{pr} (current over 15 s) of 1250 amp and 860 amp respectively, at 12 V (half the battery voltage), at 23°C ambient temperature. For Li-ion batteries, 12 V is ruled out, since the end of discharge cut-off voltage for each cell is 3 V. Therefore, with the 7S configuration, one can only drop down to 21 V. As such, 12 V is not an application platform-driven requirement. It was chosen as an industry standard based on lead acid chemistry performance specifications. For Li-ion battery, 21 V could emerge as the new standard voltage for I_{pp} and I_{pr} rating. As for the instantaneous current requirement, to match the specs of the VRLA battery, each 5 Ah LCO chemistry cell had to discharge at 312.5 amp (62.5C rate) for 0.3 s and 215 amp (43C rate) for 15 s. The 43C rate near continuous discharge is beyond the cell specs. After some research on other similar lead acid batteries in the market, typical instantaneous current requirements of a starter motor of a helicopter, and a discussion with a current helicopter industry customer, it became evident that ~1000 A for 0.3 s and ~600 A for 15 s would be sufficient. It is important to note that the focus of this program was not developing a Li-ion battery product, matching or surpassing the VRLA product specs. Therefore, a "close enough" number must be determined with respect to instantaneous current.

The 26 V, 20 Ah battery system was designed, at least with high-level considerations of FAA guidelines and certification requirements (e.g., specifications of the Technical Standard Order [TSO]-C179a; DO311A minimum operational performance standards for rechargeable lithium batteries and battery systems; and applicable UL, IEC, and UN standards such as DO-160, DO-178, DO-254, UL1642, UL2054, UN28.3, AS9100. Once again it is important to note that the focus of this program was not developing a product ready for FAA certification tests. Therefore, all these standards and guidelines were not adhered to in the strictest sense. Instead, they were used as broad guidelines.

3.3 PACKAGING TECHNOLOGY DESIGN, FABRICATION, AND DEMONSTRATION

Each cell was wrapped with the cell-packaging material to promote heat dissipation in the event of a cell failure. Keeping the airborne application in mind, the cell-packaging design focused on minimizing size and weight of the cell packs and the battery system. Various thicknesses of the packaging material were investigated. Several different cell packs were designed and fabricated, including 1S4P pack (3.7 V, 20 Ah block termed as a module for this battery), 3S4P packs (11.1 V, 20 Ah) or multi-modules, and the full-scale battery with 7S4P packs (25.9 V, 20 Ah). Each pack utilized parallel nickel tabs and series copper interconnects. Each pack was subject to various abuse conditions, including mechanical abuse (nail penetration), electrical abuse (overcharge), and thermal abuse (heating). Failure propagation results from these module and multi-modules are discussed in detail in section 4.3

Figure 8a shows an example of a 1S4P cell pack wrapped with the cell-packaging material. A total of three sets of 1S4P packs were fabricated: one with no packing material, one with 1 mm thick material, and one with 2 mm thick packaging material. Figure 8b shows a test basin used for the nail-penetration test.

(a) (b)

Figure 8. Nail-penetration abuse and failure propagation test setup; (a) 1S4P NMC cell pack with 2 mm knit cell jackets, and (b) nail penetration test basin

Several configurations of 3S4P cell packs were investigated, as shown in figure 9. The mechanical packaging configuration of these arrays were three blocks of four cells in 1S4P configuration. In terms of failure propagation testing, the 3S4P cell pack is a good intermediate representation of the entire battery. Any single cell or module-level (1S4P cell pack) failure is expected to first propagate to the next neighboring cell pack/module. Therefore, if the packaging technology prevented propagation to the neighboring module, it was expected to prevent the propagation at the full battery level. Another reason behind the choice of this 3S4P multi-module pack was dictated by the test facility at SNL. SNL's main test lab, where majority of these tests were run, has a limit of 250 Wh capacity. The 3S4P multi-module packs have an energy content of 222 Wh (11.1 V, 20 Ah), within the prescribed limit. Figure 9a shows a 3S4P block with no physical separation between the 1S4P blocks (i.e., the three blocks were physically touching each other, resulting in the most compact pack possible. Figure 9b has an insulation layer added between the 1S4P modules to reduce thermal transfer from one module (1S4P) to the next. The insulation layer shown is a 1/8″ thick G-10 plate, but the notional concept can also be fulfilled using an air gap/ physical separation between the cell blocks, only peripherally connected at the edge to provide mechanical support between the blocks. The 1S4P modules in the multi-module stacks in figures 9a and 9b use four cells stacked vertically in a 2 x 2 array. This configuration minimizes pack size while allowing the packaging technology to protect the entire pack in case of single cell failure. Figure 9c shows an alternate design with the pack laid out in a single stack configuration. Unlike the configurations shown in figures 9a and 9b, in which each cell has five neighboring cells, each cell in the configuration of figure 9c has two neighboring cells.

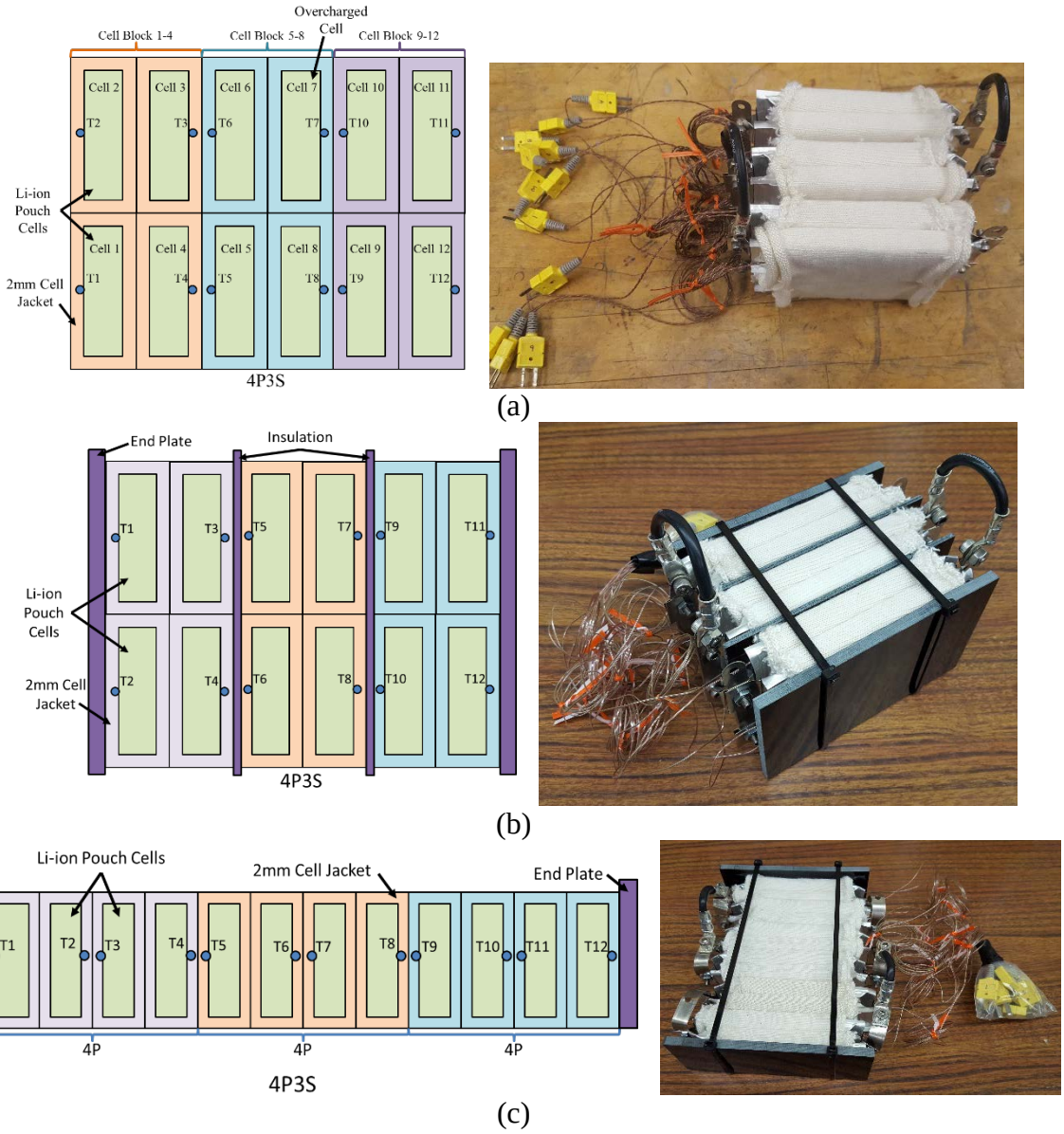

Figure 9. 3S4P pack designs for failure propagation testing: (a) design with three blocks (1S4P block) physically touching each other, resulting in the most compact pack, (b) design with similar physical layout but with air or insulation added between the 1S4P blocks, and (c) single stack 3S4P block design decreasing the number of cells surrounding each cell

For overcharge tests of the 3S4P multi-module pack, a sealed enclosure was fabricated. The box was machined from an aluminum billet and was large enough to accommodate any of the tested 3S4P cell packs. The box had an O-ring sealed lid and insulated power and instrument feedthroughs. Each 1S4P block voltage was monitored along with cell temperatures using thermistors. The box also included room for a pressure transducer and a pressure-release valve. A picture of the box is shown in figure 10 with the cell pack shown in figure 9a installed in the box.

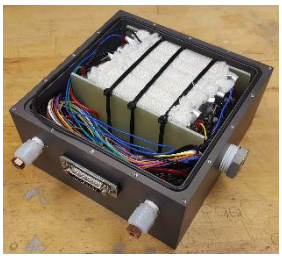

Figure 10. Machined aluminum enclosure for overcharge test of 3S4P cell pack

3.4 BATTERY SYSTEM DEVELOPMENT

3.4.1 BMS Design and Development

The 26 V, 20 Ah demonstrator battery assembled and tested in this program has a BMS, derived from the 2nd generation Trident BMS previously developed by team member Teledyne Energy Systems, Inc., but tailored towards the current battery-design requirements. It is important to note that the BMS designed and prototyped in this program is for functional demonstration purposes only and does not comply with any FAA qualification standards, such as RTCA DO178 or DO255. One of the important customizations to the BMS was the inclusion of the high current semiconductor switches that interrupt the current flow in case of a detected fault. IXYS TrenchT4 Power MOSFET IXTN660N04T4, rated at 660 A at 40 V, were used. The basic block diagram of the BMS is illustrated in figure 11.

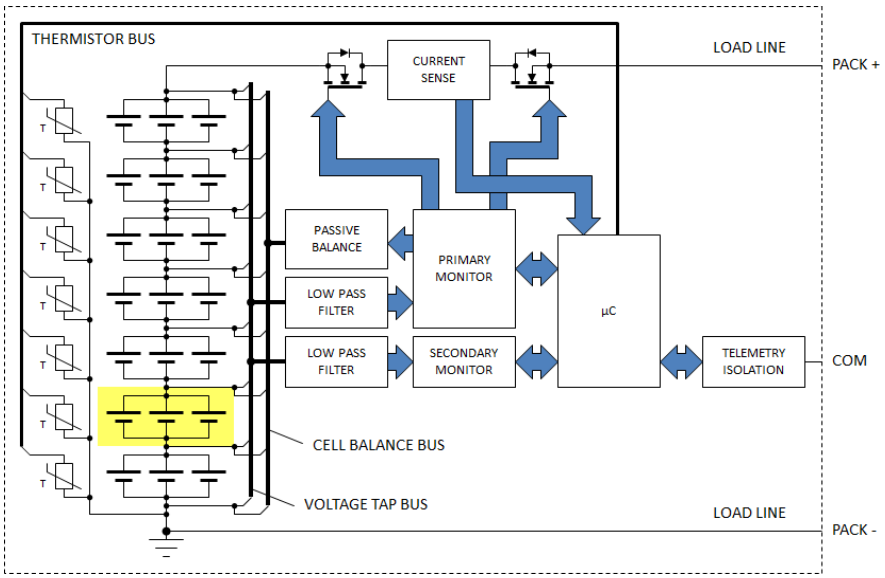

Figure 11. BMS block diagram

The BMS supports seven virtual cells strung in series. Each virtual cell consists of four cells connected in parallel, although only three are shown in figure 11. Each virtual cell includes taps for voltage monitoring and balancing. A thermistor is attached to each virtual cell for monitoring the cell surface temperatures. A primary monitoring and protection IC supervises the virtual cells during operation and contains drivers that open high-side charge/discharge MOSFETs in the event

of abusive conditions. The primary monitoring IC also controls passive cell balancing of the virtual cells. The BMS is designed to handle a 2.5% cell imbalance during a 4C charge cycle, which is a typical value. A secondary monitoring IC also monitors the cell voltages. Data from the monitoring ICs are passed to a low-power microcontroller that compares the measurements from the monitoring circuits and has authority to override the MOSFET gate drivers in the event a fault is detected. Telemetry can be broadcast to the operator through an isolated serial communication port that includes a controller area network (CAN) physical layer.

To handle the large current loads associated with a typical engine start profile, the current sense and protection electronics required modification over the current 2nd generation Trident BMS design. The current sense resistors were replaced with hall-effect current transducers. The drivers and receivers for the current sensing controllers onboard the monitoring ICs are not compatible with the hall-effect sensors, so the microcontroller now supervises the charge and discharge currents. Furthermore, the size of the MOSFETs prohibited the use of high-side and low-side redundancy, so redundant low-side protection mechanisms were omitted. Figure 12 shows a diagram of the high-side protection and current monitoring circuit. The layout consists of six parallel charge and discharge MOSFET pairs connected at the drain. Each drain connection features a current sensor so that the health of each MOSFET can be monitored. This introduces an additional fault detection capability that can be used to identify failed MOSFETs. The high side path features six parallel load paths, each independently controlled by pairs of charge/discharge MOSFETs. Each path includes a hall-effect current sensor between the charge and discharge MOSFET for current monitoring. Each path can be individually energized/de-energized to maximize the dynamic range of the hall-effect sensors in low-current conditions while maintaining adequate protection in high-current conditions. Components are rated so that a single path can temporarily handle the full 1000 A load when going from a low-current to a high-current state.

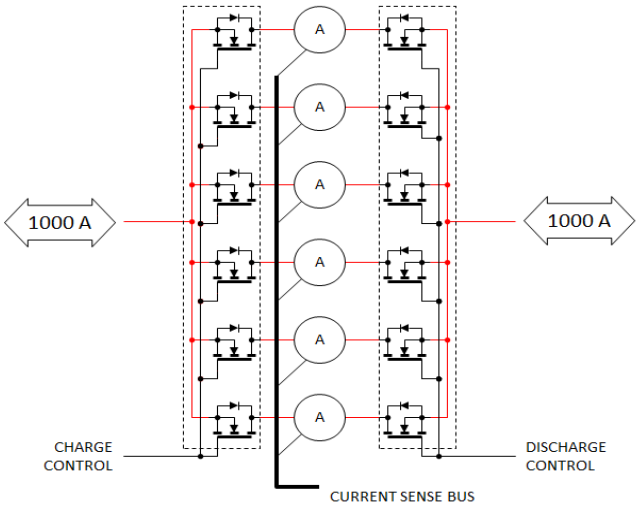

Figure 12. High-side protection and current monitoring circuitry

Overall charge/discharge gate control is shared by the primary BMS monitor and a supervisor microcontroller. The BMS monitor has authority for overvoltage, undervoltage, over-temperature, and under-temperature faults. Because the hall-effect sensors are not compatible with the current sensing of the BMS monitor chip, the supervisor microcontroller has authority for overcurrent and

short-circuit conditions. The supervisor also regulates the flow through the individual paths and is capable of detecting MOSFET gate failures too. Figures 13a, 13b, and 13c show the completed main BMS board, the high-side MOSFET interface board, and the driver board for the high-side switch respectively.

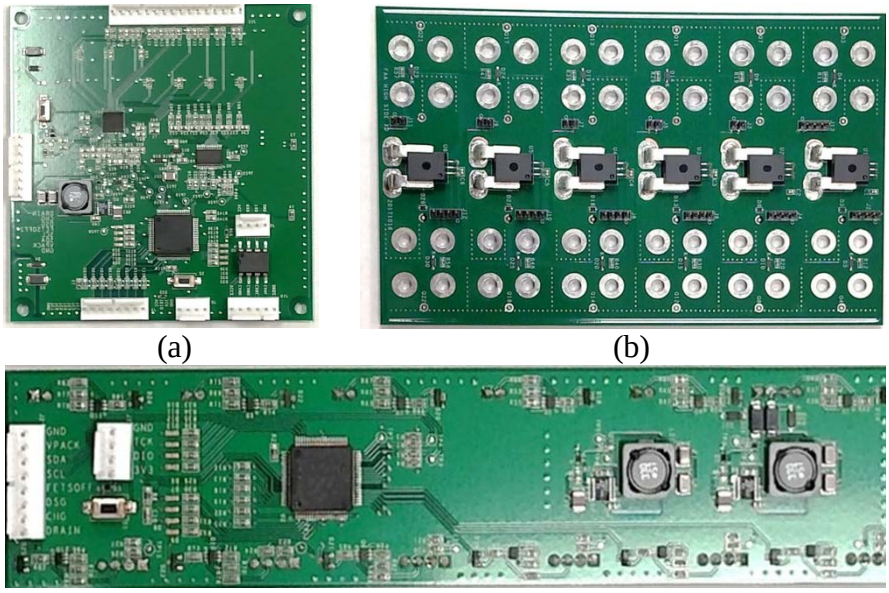

Figure 13. Completed Li-ion BMS printed circuit boards: (a) main board, (b) charge/discharge gate interface and current monitor board, and (c) charge/discharge gate driver board power

A second iteration of BMS design was performed after the initial board checkout and functional testing. The first improvement was to refine the high-side MOSFET drivers for the charge and discharge gate controllers, to take advantage of a high-side driver on a single chip that reduced the total parts count and improved the overall performance of the system. Adapters were fabricated to use the new high-side controllers with the electronics that were previously fabricated for the high-side driver PCB and the high-side interface PCB. Figure 14 shows the hardware with the updated high-side controllers along with the adapter boards that were used in the final prototype.

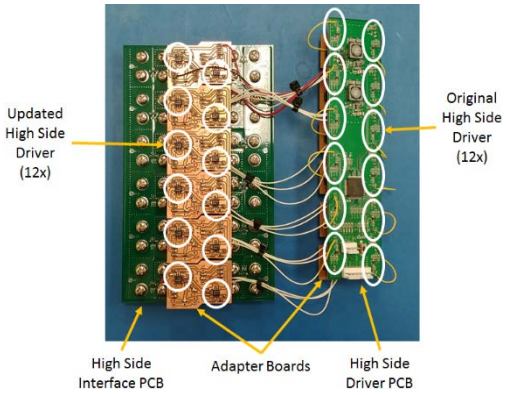

Figure 14. Updated high-side MOSFET drivers for charge and discharge gate controllers

The block diagram of the original BMS is shown in figure 15. The BMS was designed to be completely self-contained, so the baseline design derived power for all circuits from the cell stack. An onboard DC/DC converter converted the stack voltage to a lower level for powering the microcontroller, CAN transceiver, and debugging peripheral circuits. The combined draw from these circuits is typically 10-15 mA, even when the battery is not being charged or discharged. During the second design iteration, this was deemed too high. Therefore, power-saving capabilities were implemented in the BMS circuit to reduce the discharge load on the cell stack. To do this, the system block diagram was modified.

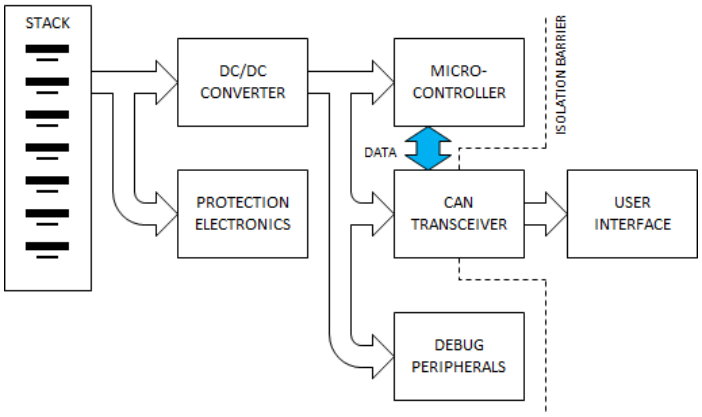

Figure 15. BMS block diagram with debug peripherals and CAN transceiver run by battery

A voltage supervisor was inserted between the stack and the DC/DC converter. If the cell voltage dropped below 0% state of charge (SOC), the other circuits were disabled and remained dormant until a charge was applied. For safety reasons, the protection electronics continued to draw power from the stack at all times, ensuring that they were constantly powered and monitoring the battery. These changes reduced the quiescent load to less than 0.5 mA. Furthermore, an isolated DC/DC converter was included so the CAN transceiver circuit receives its power from an external source. This eliminated the draw of the CAN transceiver from the stack, which can be as high as 100 mA when transmitting. Lastly, the circuits that were used for debugging the boards while bench testing have been disabled because they are no longer needed once the BMS is added to the battery box and the battery box is sealed. The final BMS block diagram implementing the power-saving modifications is shown in figure 16.

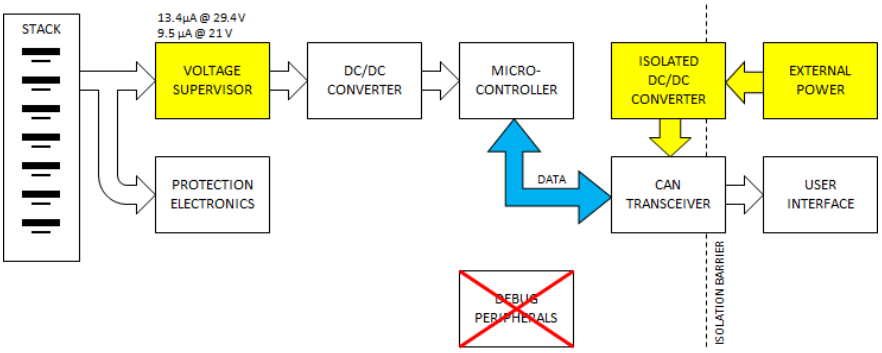

Figure 16. Upgraded BMS block diagram with voltage supervisor included, debug peripherals disabled, and CAN transceiver run by external power

The first BMS board modification prototyped, shown in figure 17, incorporates the capability for externally powering the CAN transceiver. An isolated DC/DC converter provided galvanic isolation between the user supply and the stack. The second modification, shown in figure 18, incorporates a voltage supervisor on the voltage regulation circuit that powers the microcontroller and peripheral circuits on the BMS. The voltage supervisor was tuned so that the output of the voltage regulator was disabled whenever the stack voltage dropped below a defined set point. While the voltage regulator output was disabled, the safety monitoring circuits would continue to function, but the microcontroller would be powered down until a charging load is applied.

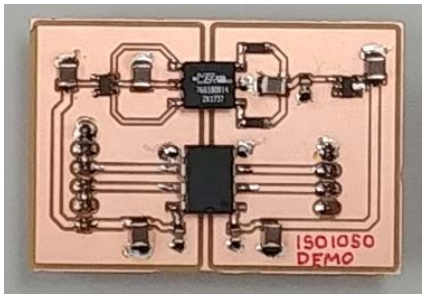

Figure 17. Prototyped CAN transceiver with external power modification

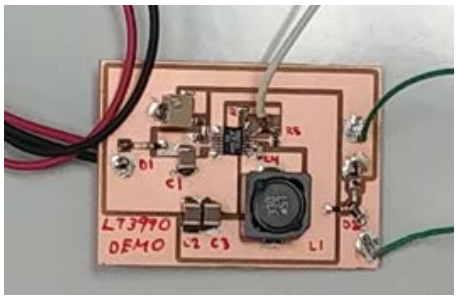

Figure 18. Prototyped voltage regulator with voltage supervisor circuit

For the demonstration prototype, the power down threshold was tuned to 20 V, and a 0.5 mA load was attached to the output. While the stack voltage remained above 20 V, the regulator was enabled, and the full load was delivered to the output. Once the stack voltage dropped to 20 V, the output was disabled, and the total system load decreased to less than 10 µA. Below 20 V, the total load on the stack was the combination of the load through the supervisor circuit and a small quiescent load through the voltage regulator. Performance data of the voltage supervisor are shown in figure 19.

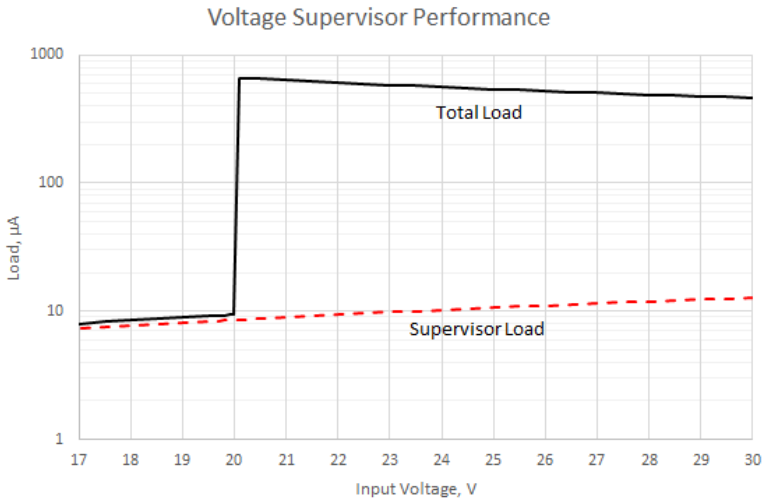

Figure 19. Performance data for the voltage supervisor

All these improvements were prototyped at component level, tested, and implemented in the Rev 2 BMS design. New PCBs were fabricated and tested. A graphical user interface (GUI) was also developed to manage the BMS telemetry and debug the complete system. Figure 20 shows a screen capture of the BMS utility running on a Microsoft® Windows® laptop.

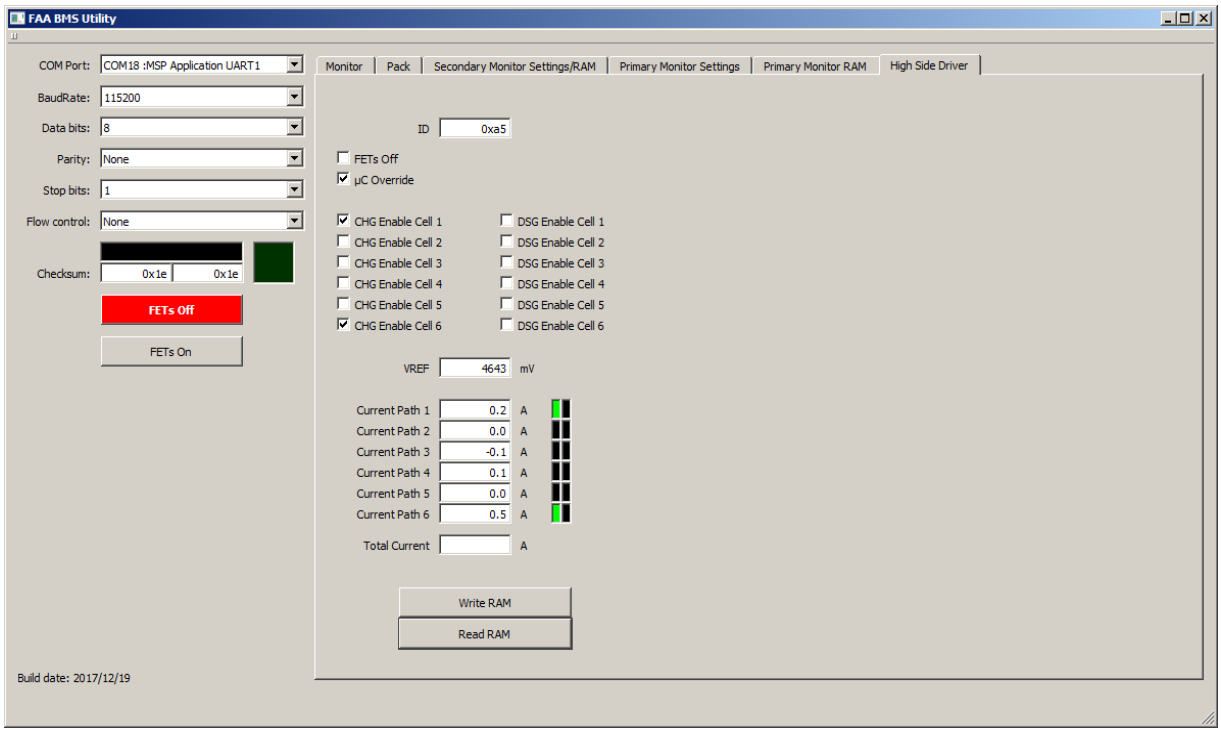

Figure 20. Screen capture of the BMS GUI utility that will be used to monitor and control the FAA demonstration module

3.4.2 Battery System Design and Fabrication

Based on the system definition and specifications laid out in table 2 in section 3.2, a 7S4P cell pack was designed for the 26 V, 20 Ah full battery. Figure 21 shows the final pack design along with major features. Each cell was equipped with 2 mm thick packaging material. Keeping the size and weight constraints of the airborne platform in mind, it is best to keep the thickness of the packaging material as low as possible. Section 4.2 shows the tested failure propagation process with 1-mm thick packaging material. It was not enough to prevent the cell-to-cell failure propagation. Therefore, 2 mm thickness was selected. The four (electrically) parallel cell pack (1S4P configuration) was created by bolting cells to two nickel tabs. Seven 4P packs were then connected in series using copper interconnects. All series and parallel connections were made with solid brass hardware. The final pack weight was calculated to be 4.5 kg, resulting in a cell pack energy density and power density of 109 Wh/kg and 5.5 kW/kg, respectively. The battery pack was placed in a two-chamber, machined aluminum battery box. The light-weight metal casing was chosen to ensure rigidity and strength to handle pressure rise due to failure propagation, if any. The bottom among the two chambers would contain the cell pack and the packaging technology, and will be sealed. The top chamber would house the BMS and solid-state MOSFET switches. This arrangement would place the control switches and control electronics away from the cells where they would not be damaged in the case of a thermal runaway. Sealed feedthroughs would be placed between the two chambers allowing transfer of power along with communication of pack voltages and cell temperatures. In addition to the electrical feedthroughs, the BMS chamber would also integrate a pressure-release system. The final component of the battery box would be

the lid, which contains all external connections including power, communication, and the vent port.

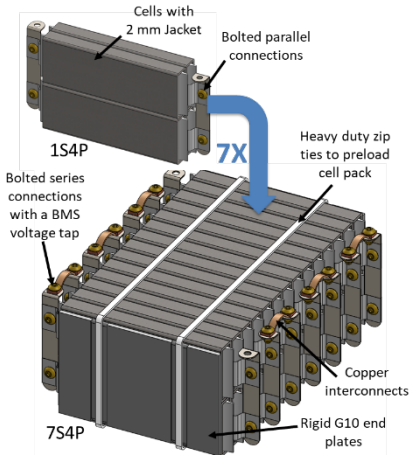

Figure 21. 26 V, 20 Ah battery pack equipped with the packaging technology

Because the final intent (beyond the scope of this program) was to create a Li-ion version of TBP's current VRLA product 7246-20, the overall footprint and design of the Li-ion battery box were chosen to match the current VRLA battery. One of the major changes in the design compared to that of the VRLA is shortening of the height of the battery box to include a secondary compartment that would contain the BMS and power electronics. The BMS board has mostly low-power components. The high-power MOSFETs, which would be used to interrupt current in the case of a fault, would be mounted to the underside of the top lid. The aluminum box lid would act as a heat sink to ensure the junction temperature for the MOSFET devices stayed below the manufacturer-suggested temperature of 100°C to ensure full device life expectancy.

A pressure-release valve was designed to release the effluents in case of a cell failure inside the battery compartment. In the first design, a modified 1″ NPT fitting and a modified 1″-12 set screw were considered to create a seal disk whose burst pressure could be adjusted by altering the disk material and thickness, as shown in figure 22. However, the part was large and heavy, and relied on an additional O-ring seal, a potential leak point. To circumvent this issue, a design was chosen that incorporated the burst disk directly in the metal lid of the battery box chamber. This would be accomplished by thinning down a section of the aluminum box lid to a specific thickness to achieve a desired burst pressure. The area of the sections could be adjusted to change the failure pressure point. A stress riser (groove pattern) could also be scored or engraved into the back prior to thinning, enabling capability to tune the burst pressure without any additional sealing. Figure 23a shows the updated burst disk setup, showing a 0.25″-thick aluminum plate with an area thinned down to 0.030″ thick. The thin area also had a stress riser engraved into the back side. Figure 23b shows a simple finite element analysis (FEA) of the burst disk plate using SolidWorks' built in capability. A 30-psi pressure was applied to the front side of the plate whereas the back side was fixed. All areas shown in red signify zones where the factor of safety (FoS) is less than 1 (minimum FoS is 0.955). The simulation shows that this burst disk design should fail and release pressure at ~ 30 psi.

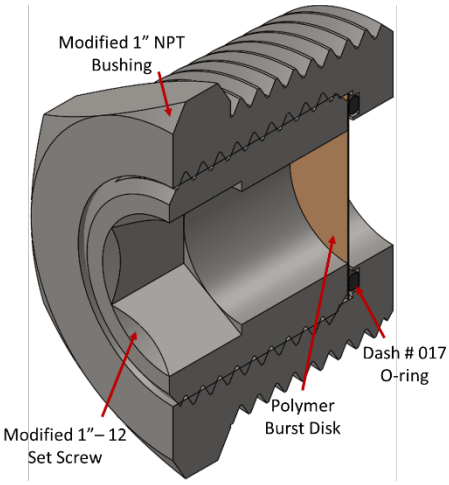

Figure 22. Original burst disk pressure release assembly design using commercial-off-the-shelf parts

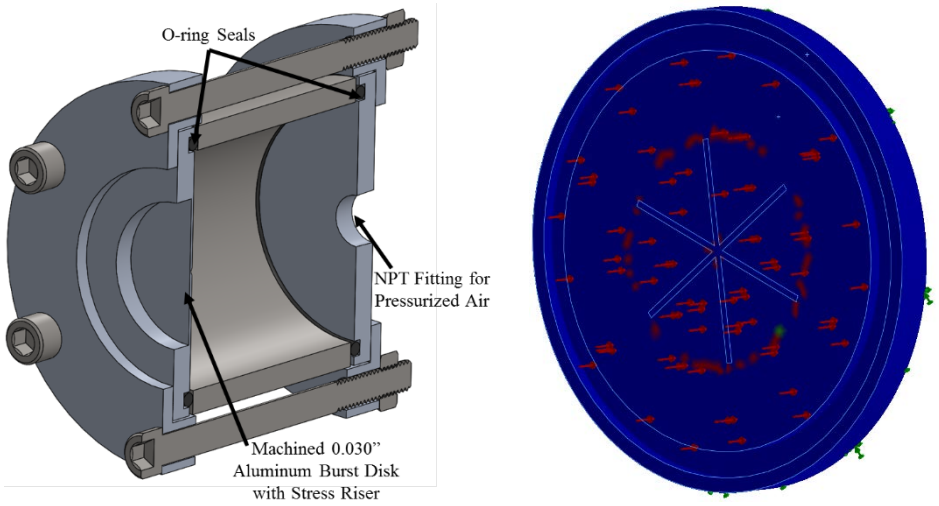

Figure 23. Pressure release burst disk assembly integrated directly to aluminum plate: (a) sectioned view of the design, (b) FEA results for 30 psi on the aluminum burst disk plate with engraved stress riser shown; all areas shown in red signify zones where the FoS is less than 1 (minimum FoS is 0.955)

Based on the SolidWorks FEA model, the burst disk shown in figure 23a was fabricated and tested. Pressurized nitrogen was slowly applied through the threaded NPT fitting, and the internal pressure was monitored with a pressure gauge to observe the pressure at which the disk failed. The experimental results showed that the disk survived in excess of 100 psi, far exceeding the model results. Clearly, this would not serve the purpose. Reexamination of the model revealed that the mesh size resolution of SolidWorks' built-in FEA model is not sufficient to accurately capture the stress in the small, 0.03″ (750 μm) thickness. Although there is a high-fidelity FEA modeling capability in house with ANSYS multi-physics, the resources were not available to conduct extensive modeling. Instead, the focus was on experimentation, and the burst disk was refabricated using a weaker aluminum alloy (3003 H14 vs. 6061 T6) and reducing the disk thickness to 0.025″

(625 μm), the lowest allowed thickness due to machining limitation. This resulted in an average burst pressure of 87 psi in two samples. Subsequently, a commercially available product provided by Zook^{TM} was investigated. The disk is a carbon composite with a designed burst pressure of 50 psi. The disk is mounted between standard KF flanges, creating a hermetic seal, and releases pressure at the design point. This product looked promising, but the mounting method was far too bulky for this applications. In the end, a commercial-off-the-shelf adjustable spring-loaded pressure-release valve was chosen to release pressure buildup in the battery chamber. As is shown in the safety testing results in section 4, venting and release is an area that needs further design, testing, and characterization.

Figure 24 shows the complete design of the 26 V, 20 Ah demonstrator battery along with details of the enclosure assembly. The final size and weight specifications are listed in table 2.

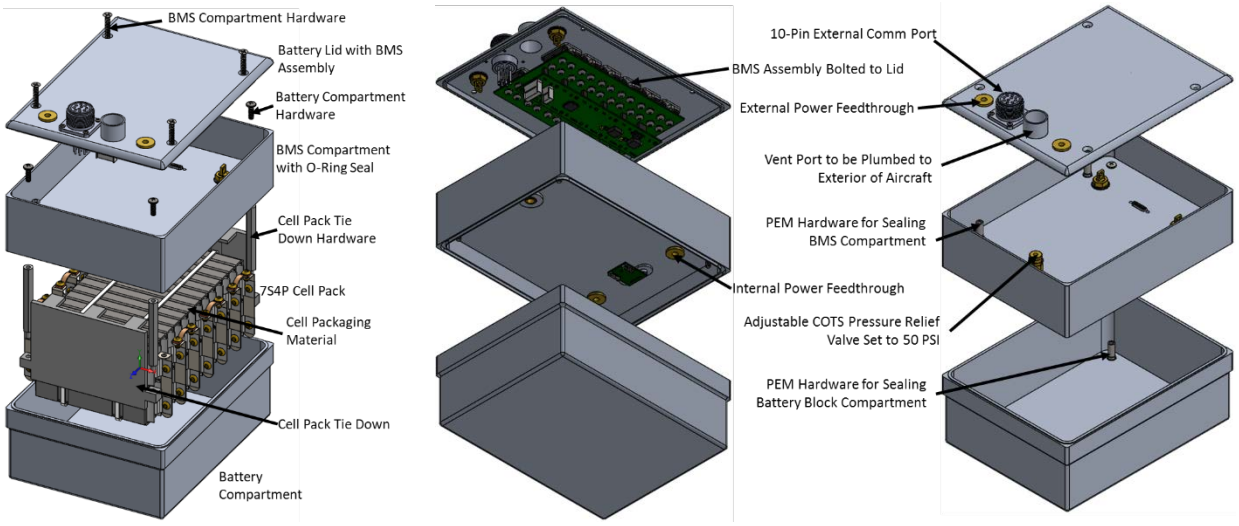

(a) (b)

Figure 24. 26 V, 20 Ah Li-ion aircraft starter battery, the demonstration platform of this program incorporating the packaging technology: (a) exploded view, (b) box assembly detail view

3.5 BATTERY ASSEMBLY

Based on the components (cell pack, enclosure, wiring, valve, and BMS) described in the previous sections and the battery design, four prototype units of the 26 V, 2 Ah battery were assembled (figure 25). Two of these units were fully equipped with the BMS and were used for functional testing. Two of these units were fully equipped with the BMS and were used for functional testing (e.g., helicopter starting profile discharging). The other two contained the same battery pack but were not equipped with a BMS. These units were sent to team member SNL for failure propagation testing in BMS-disabled conditions. Figure 25 shows one of the completed batteries. The high-power brass power terminals are visible on the top of the battery along with the communication port capable of transmitting the battery status and BMS readings, including cell voltages, temperatures, discharge current, etc. to the aircraft in CAN Bus. In addition to the power terminals

and comm. port, the top also has a large vent port that is designed to release internal battery pressure and effluence in the case of an internal failure.

Figure 25. Fully 26 V, 20 Ah prototype Li-ion battery with packaging technology and BMS

3.6 FUNCTIONAL TESTING

Functional testing was performed on the assembled batteries. The first set of tests was to characterize the instantaneous current rating; that is, I_{pp} (current over 0.3 s) and I_{pr} (current over 15 s) at a constant 21 V. Figure 26a shows the battery voltage and discharge current. The measured values of I_{pp} and I_{pr} were 756 amps and 403 amps respectively. These results were lower than anticipated from the projection of the single cell-level tests shown in figure 6. This could be due to the voltage drop in the internal battery wiring and the high-power semiconductor switches in the BMS. This could be further optimized in the future. Figure 26b shows the corresponding rise in average cell temperature. The packaging technology ensures a nominal ~7°C temperature rise in spite of the high current discharge.

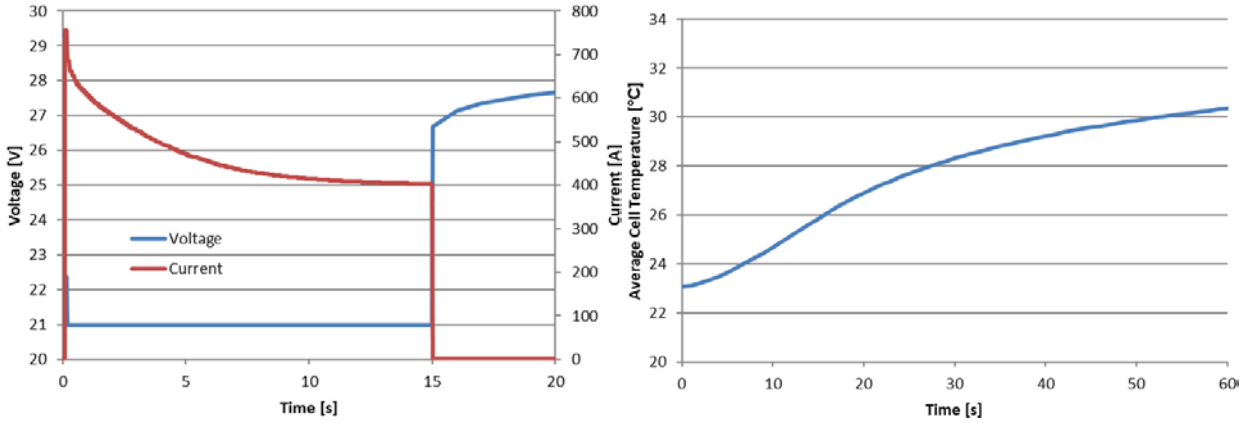

(a) (b)

Figure 26. I_{pp}–I_{pr} discharge test results: (a) battery voltage and discharge current and (b) average cell temperature during and after discharge testing

The battery was also discharged in an engine starter profile for a small helicopter (figure 27a). At the peak starting current of 577 amps, the battery voltage dropped to 23.1 V. Figure 27b shows the corresponding average cell temperature rise, ~3°C.

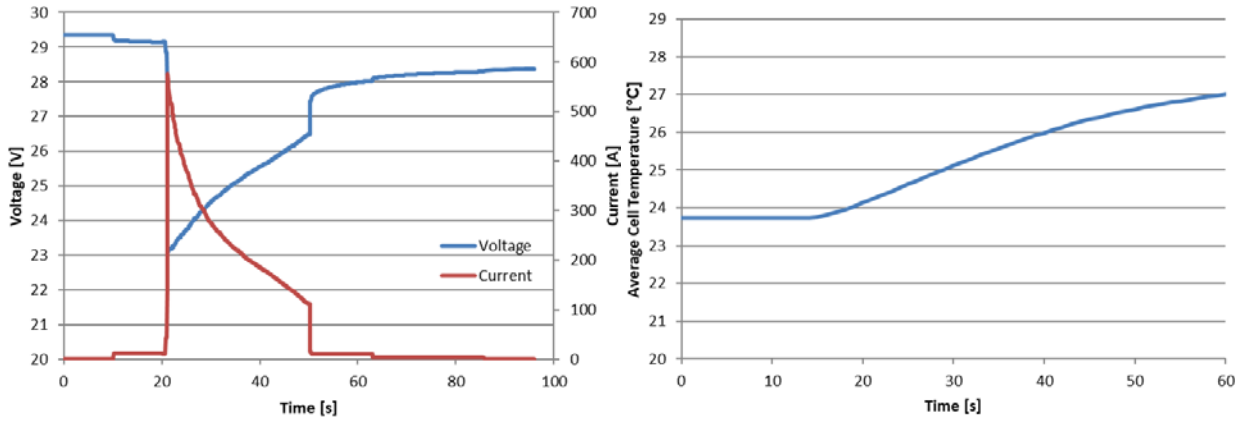

(a) (b)

Figure 27. Helicopter engine start discharge profile test results: (a) battery voltage and discharge current and (b) average cell temperature during and after discharge testing

4. SAFETY CHARACTERIZATION AND TESTING

All safety characterization tests (i.e., cell failure, cell-to-cell failure propagation, and total catastrophic failure of the entire battery, if any) were conducted at team member SNL's test facility. Safety characterization of the packaging technology, that is its effectiveness in preventing failure propagation, was established in a step-by-step method, first starting at single cell-level, then moving up to module and multi-module-level, and finally into the full scale 26 V, 20 Ah battery level. Three different trigger mechanisms or abuse conditions were tested: electrical abuse (overcharge), mechanical abuse (nail penetration), and thermal abuse (external heating). These tests were conducted following SNL's standardized propagation testing methodologies for multi-cell batteries, outlined in SAND-2014-17053[1].

4.1 SINGLE CELL-LEVEL SAFETY CHARACTERIZATION

The first set of tests were conducted at single cell-level (Kokam SLPB11543140H5 pouch cell). The objectives were to identify reliable thermal runaway trigger mechanism(s) and to establish whether the cell fails against that trigger mechanism and the magnitude of the event. For each of the three types of abuse conditions listed above, two tests (on two different cells) were carried out for repeatability. The single cell-level test results are summarized in table 3.

[1] Orendorff, C.J., Lamb, J., Steele, L.A.M., and Spangler, S.W., "Propagation Testing Multi-Cell Batteries", SAND-2014-17053, Albuquerque, NM, Oct 2014

Table 3. Summary of single cell-level abuse test results: EUCAR is a failure rating system, 4 indicates heavy smoke and venting, and 5 indicates visible ignition of the battery

Cell	Test	Condition	End Condition	Notes	EUCAR
001	Thermal ramp	100% SOC heated at 5°C/min	250°C, hold for 15 min or failure	Vent and heavy smoke; no self-ignition	4
002	Thermal ramp	100% SOC heated at 5°C/min	250°C, hold for 15 min or failure	Vent and heavy smoke; no self-ignition	4
003	Overcharge	1C (5A), room temperature	250% SOC, hold for 15 min or failure	Incandescent particle release and self-ignition	5
004	Overcharge	1C (5A), room temperature	250% SOC, hold for 15 min or failure	Incandescent particle release and self-ignition	5
005	Sharp nail into edge	3 mm rod, 2 cm/s, room temperature, 100% SOC	Failure; full penetration	Vent and heavy smoke; no self-ignition	4
006	Sharp nail into edge	3 mm rod, 2 cm/s, room temperature, 100% SOC	Failure; full penetration	Vent and heavy smoke; no self-ignition	4

Thermal runaway was observed for all tests with a failure severity of at least EUCAR 4. Overcharge abuse testing was more severe in both tested cells, with incandescent particle release and self-ignition of the vent gases during thermal runaway. Temperature rise data for each type of trigger mechanism is shown in figure 28. Depending on the trigger mechanism, the maximum cell temperature reached between 300 to 500°C.

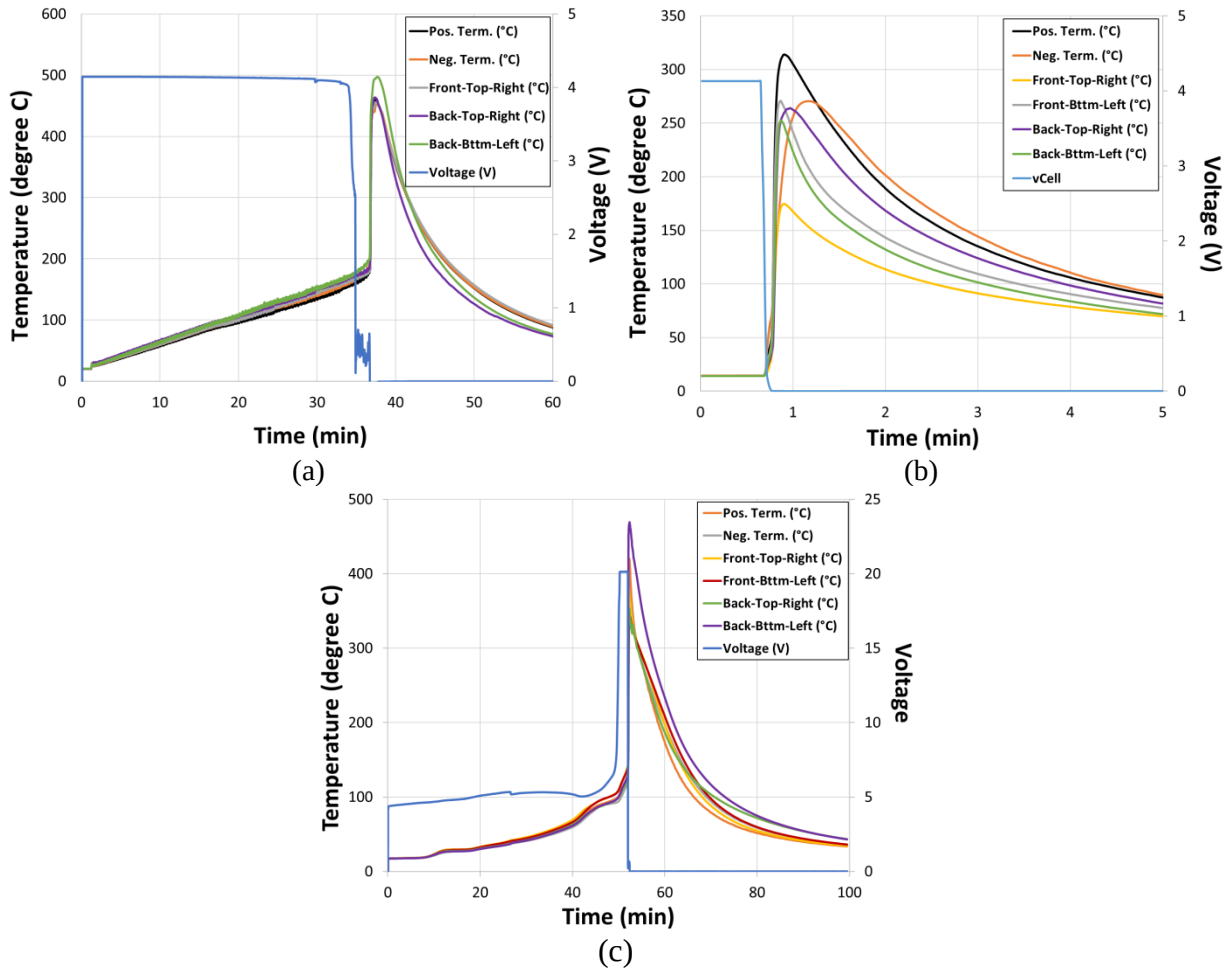

Figure 28. Cell temperature and voltage during single-cell abuse tests: a) thermal/ overheating failure test with a resistive heater; b) edge nail penetration abuse test; and c) electrical overcharge abuse test

Failure of the single cell under all abuse conditions and the resulting high temperature proved the volatility of the LCO cell chemistry and underscored the importance of a safety mechanism to prevent catastrophic failure propagating across cell banks. Under this program, no single cell-level test was conducted with the packaging technology. The technology is designed to prevent cell-to-cell failure propagation, not single cell failure. However, presence of the packaging technology, even at the single cell-level, is expected to substantially lower the cell case temperature and, therefore, the autocatalytic reaction, generating more heat.

4.2 MODULE-LEVEL SAFETY CHARACTERIZATION

The module, as defined earlier in the report, is a four-cell block in 1S4P configuration. The 3.7 V, 20 Ah 1S4P block forms the repetitive building block of the 26 V, 20 Ah full-scale battery. Although the single cell was shown to fail under all three abuse conditions, for the purpose of the module-level test, the focus was on only nail penetration and overcharge tests. In the previous AFRL-funded HESM Phase I work with 26650 LFP cell, it was proven that it is very difficult to trigger a runaway by thermal abuse (overheating of a cell) in presence of the packaging

technology[2]. The cooling functionality of the technology keeps the cell temperature low enough that failure could not be triggered by overheating, unless the heat input was substantially increased. That would require a much higher power rating and larger heater. Such a trigger mechanism may not be realistic and relevant.

Module-Level Nail Penetration Testing: Three module-level nail penetration tests were conducted: one module without the packaging technology (baseline), one module with a 1-mm-thick packaging material, and the last module with a 2-mm-thick packaging material around each cell. In all these experiments, a local cell failure was triggered by the nail penetration, and the propagation of that failure to the remaining cells of the module was monitored. Figure 29 shows a schematic picture of the four-cell stack configuration for these tests and the location of the nail penetration. From the effectiveness of the packaging technology standpoint, the bottom two cells are easier to cool. Therefore, either of the upper two cells in the stack pose the worst-case scenario for triggering the failure and allowing the propagation. Furthermore, from an experimental setup standpoint, it is easier to penetrate the upper cell. The cell packs were placed in a test basin, and a 3-mm blunt nail was used for failure initiation. A total of six thermocouples were placed on the cell packs, directly in contact with the cells' walls, as shown in the schematic of figure 29. Figure 30 shows the test setup and the module voltage/temperature results for the module without the packaging technology (baseline).

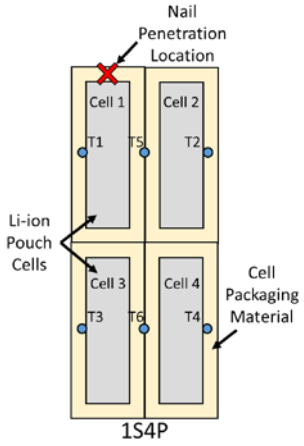

Figure 29. 1S4P cell pack nail-penetration test setup

[2] Bhunia, A., Gould, K.D., Cai, S.Q., Sudre, O., Hodge, J.D., Lamb, J.H., Orendorff, C.J., and Saunders, J.H., "Hybrid Energy Storage Module Militarized Energy Storage Device Structure. Task Order 001: Proof-of-Concept Demonstration of Multi-Functional Jacket for Thermal Management and Runaway Prevention of Lithium-ion Batteries," AFRL Report, March 2018.

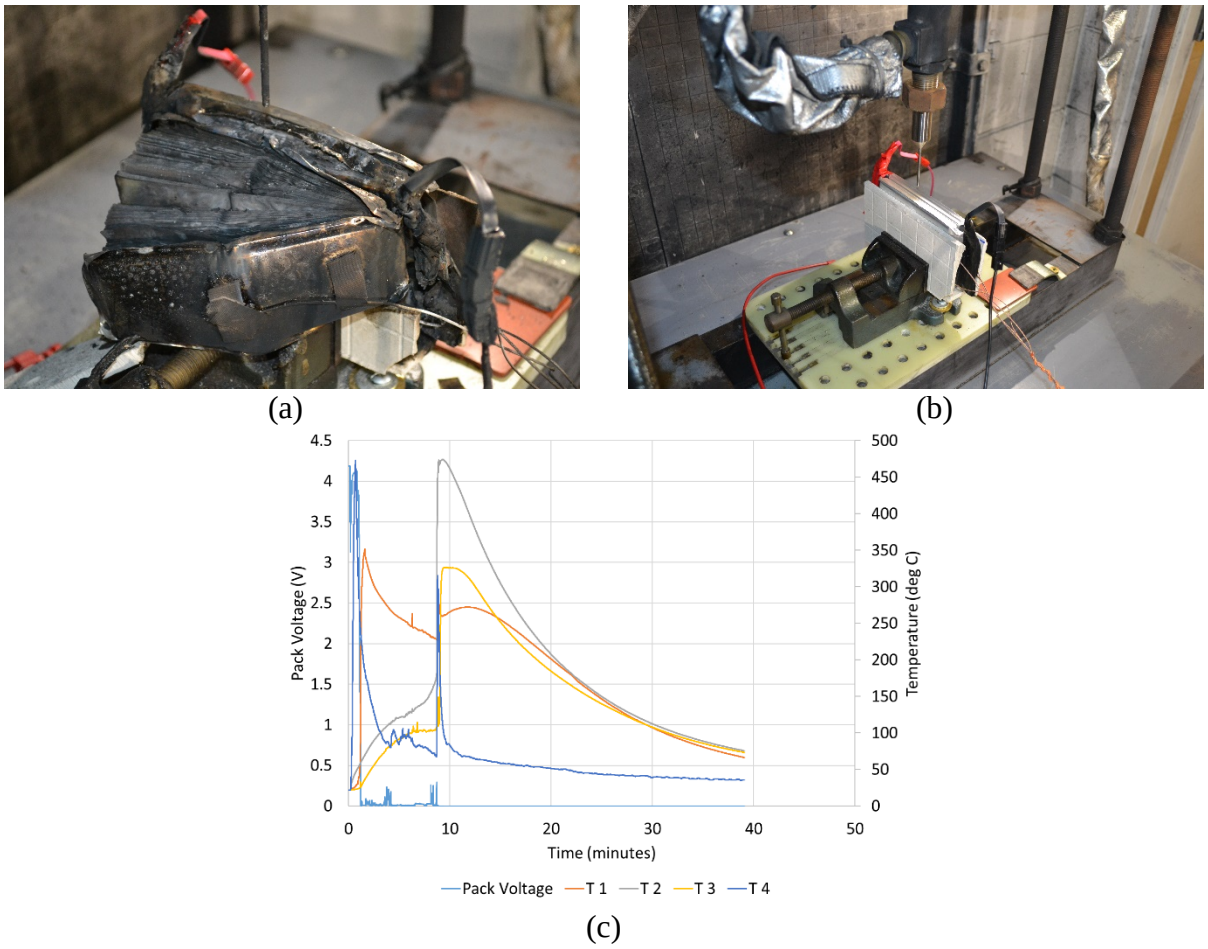

Figure 30. Mechanical abuse and failure propagation test for a 1S4P cell pack (module) without the packaging technology (baseline): (a) cell pack and test setup, (b) cell array after the thermal runaway event, and (c) voltage and temperature results

The initial cell failure was observed immediately after penetration into the side of a single upper cell. An immediate voltage loss and self-ignition was also observed with this event. Some initial propagation was observed, however the main propagation event occurred at ~8.5 minutes, where a significant thermal runaway event including a momentary large fireball consumed the remainder of the pack. Peak temperatures of up to ~475 °C were observed during this event. It is suspected that the thermocouple did not record the actual peak temperature, particularly of the flame during the final thermal runaway, which was likely much higher.

Figure 31 shows the test results (cell case temperature measurements and the pack voltage) for the two modules incorporating the packaging material, one with 1 mm thickness and another 2 mm. The initial penetration caused a hard short circuit failure of cell 1, the penetrated cell, and both packs' penetrated cell reached in excess of 400 °C.

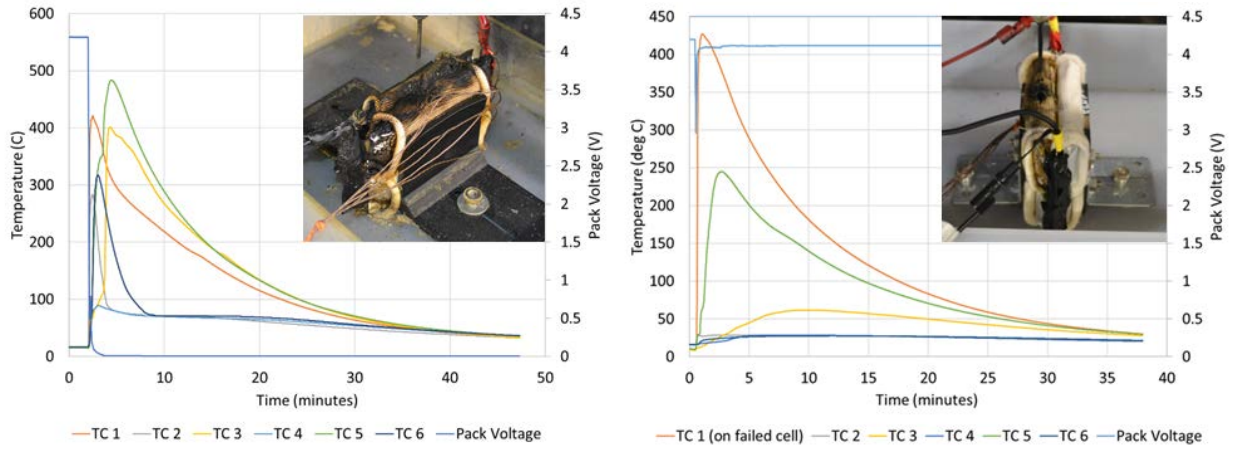

(a) (b)

Figure 31. Cell temperature and voltage during 1S4P cell pack nail penetration testing: (a) 1 mm thick cell packaging material; and (b) 2 mm thick cell packaging material

For the cell pack equipped with 1-mm-thick packaging material, the adjacent cell (cell 2 in figure 29), also went into immediate thermal runaway. The cell directly below the penetrated cell (cell 3) also went into thermal runaway after ~2.5 minutes. The maximum pack temperature reached 480°C. The remaining bottom-right cell, furthest from the penetrated cell, did survive. It had severe swelling, but showed no signs of venting. The cell pack with 2 mm packaging material prevented the cell failure propagation and maintained the neighboring cell temperatures at ~50°C or lower.

The 1-mm packaging material thickness test had a few irregularities that were not observed in the nail penetration test with 2 mm packaging. The first one being complete loss of pack voltage. The internal fused tab in all four cells was triggered, meaning that all four cells experienced significant (> 250 A) short circuit current. This electrical shorting of all cells may have played a role in the failure of the neighboring cells. In the 2 mm thickness test, the penetrated cell lost internal connectivity immediately which protected the neighboring cells from short circuit current. In addition to the electrical anomaly, there were also difficulties triggering the initial failure of the target cell during the 1 mm thickness test. Failure was only observed after a total nail displacement of 60 mm from the starting position, providing some potential for impacting cell 3. A post mortem of the pack was performed to determine the extent of this condition and what role it may have played in the failure propagation. Initial inspection did not show apparent penetration; however, inspection of the inner electrode layers showed that compression of some of the electrodes did occur as result of the extended penetration. It is not believed that was the main cause of the cell failure because of the two and half minute delay between the nail penetration and the failure of cell 3. The additional compression during the failure may have created additional thermal contact, along with close proximity to the nail providing an alternate means of thermal conduction. Figure 32 shows images of both lower cells: the cell impacted by over-penetration (figure 32a) and the surviving cell (figure 32b).

(a) (b)

Figure 32. Cell pack tear-down after mechanical abuse and failure propagation test for a 1S4P cell pack with 1 mm thick packaging materials: (a) failed cell with electrode compression damage due to over penetration of the nail and (b) surviving cell exhibiting swelling but no venting

Module-Level Overcharge Testing: An overcharge test was performed on the 1S4P cell pack, equipped with a 1-mm-thick packaging material. The cells were placed in the test basin, and the pack was subjected to a 1C (5 A) overcharge until cell failure was initiated. The cell and thermocouple arrangement were the same as shown in figure 29. Being in electrically parallel configuration, the overcharge current was applied to all four cells in the pack. The charge was applied for 34 minutes with the pack voltage reaching ~5.5 V before cell failure was observed. Figure 33a shows the result for the module incorporating the packaging technology. All four cells failed with thermocouple 5 reaching a maximum temperature of ~600°C, while thermocouples 2, 4, and 6 stayed below 50°C. In comparison, for the baseline case (module without the packaging technology) shown in figure 33b, temperature of all the cells exceeded 600°C with the hottest cell reaching over 1000°C.

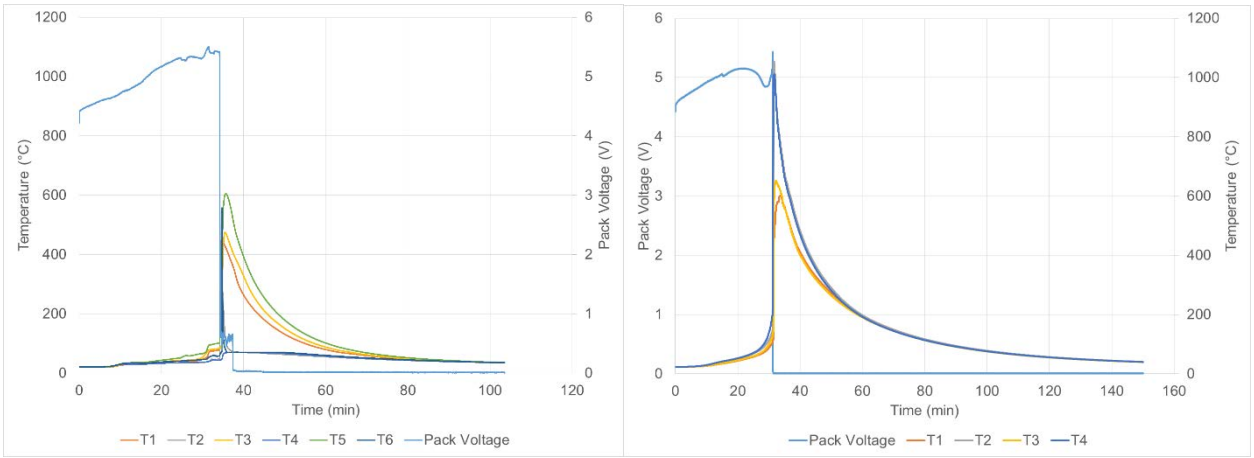

(a) (b)

Figure 33. Overcharge failure test results for a 1S4P cell pack; (a) Teledyne's packaging technology results and (b) baseline results

Conclusions from module-level safety characterization: The results presented in this section indicate that if a single cell of the four-cell module (in 1S4P configuration) failed, such as by nail penetration, the packaging technology can substantially prevent any cell-to-cell failure propagation. If the entire module fails, such as by electrical overcharge, the packaging technology

cannot prevent the module-level failure, but it can drastically reduce the peak temperature, which would help mitigate further propagation to the neighboring modules.

4.3 MULTI MODULE-LEVEL SAFETY CHARACTERIZATION

The next logical step was to investigate how failure propagates from one module to the neighboring modules. For this purpose, a three-module pack was built, a stack of 12 cells in 3S4P electrical configuration. Figure 34a shows one implementation of the 3-modules. If a cell in the middle module, or if the entire middle module went into runaway, that would create a worst-case scenario because there are two potentially vulnerable, neighboring modules.

Multi Module-Level Nail Penetration Testing: Figure 34a shows a schematic of the 3-module stack in 3S4P configuration, equipped with 2-mm-thick packaging material on each of the 12 cells. A thermal runaway was initiated on Cell # 7 by nail penetration. Cell #7 or #8 poses the worst-case scenario in this configuration because: (a) any of the upper cells are more difficult to cool in this vertical two-stack configuration; (b) both these cells belong to the middle of the three modules; and (c) both these cells are surrounded by five neighboring cells, which are potentially vulnerable to propagation. K-type thermocouples were used to monitor the cell temperatures during testing. As shown in figure 34b, temperature of cell #7 rapidly reached ~410 °C. The accompanying video showed heavy outgassing. However, there was no propagation to the neighboring cells. A neighboring cell (Cell 8) was observed to reach only ~50 °C. Other cells showed only a small rise above ambient temperature with none surpassing 30°C. No signs of latent failure were observed over a 3-hour time window.

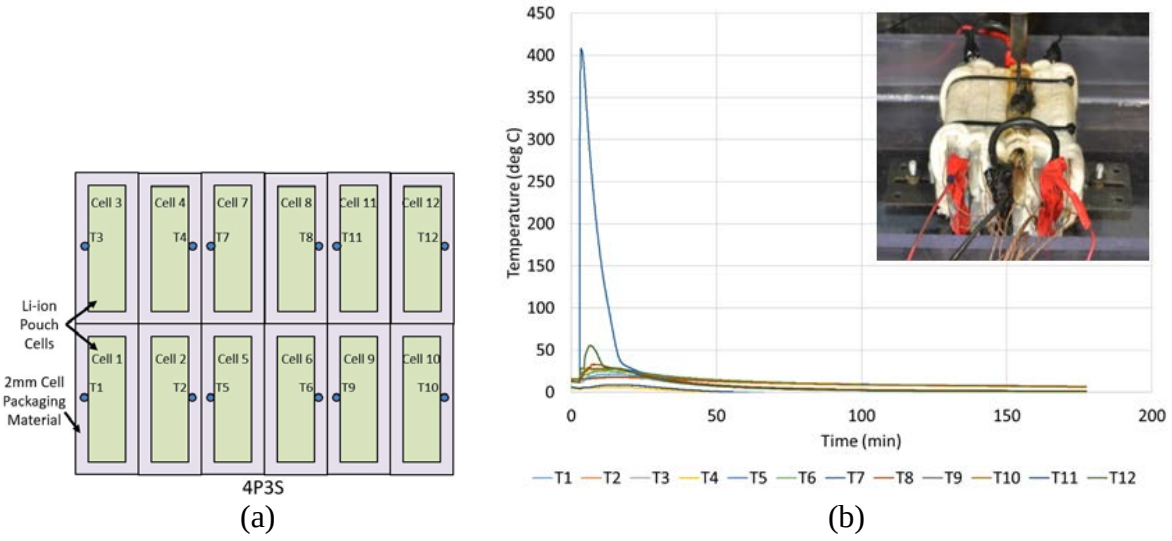

Figure 34. Results for nail penetration failure propagation testing on multi-modules (3 modules in a 3S4P cell pack): (a) cell and thermocouple locations and (b) cell temperatures during nail penetration

Multi Module-Level Overcharge Testing: Based on the results presented so far, this test would be the real worst-case scenario. As in an overcharge failure, all four cells of a module take off, releasing energy content of 20 Ah cells (4 each of 5 Ah). These tests were carried out in three different module stacking configurations, discussed in figure 9 (section 3.3). Each of the packs

was equipped with 2-mm-thick packaging material. Figure 35 shows one of the test setups, corresponding to the pack configuration shown in figure 9a. Overcharging the middle module of this three-module stack resulted in peak cell temperatures of 600°C and failure propagation to both the neighboring modules. On the cell pack with additional insulation material between the modules (figure 9b), the peak cell temperature on the failed module reached ~450°C while the cell temperatures in adjacent modules stayed well below the auto-ignition temperature of 150°C, resulting in no failure propagation. For the multi-module configuration of figure 9c, failure propagated to the end modules, although it was not a full thermal runaway. The effectiveness of the packaging technology somewhat mitigated the catastrophic failure. For example, the temperature of the failed cells of the neighboring module ranged between 180°C and 500°C (in configuration 9c), compared to ~300 – 600°C in the previous test with dual stack cells (configuration 9a). The temperature data for all the multi-module overcharge tests for all three configurations are shown in figure 36.

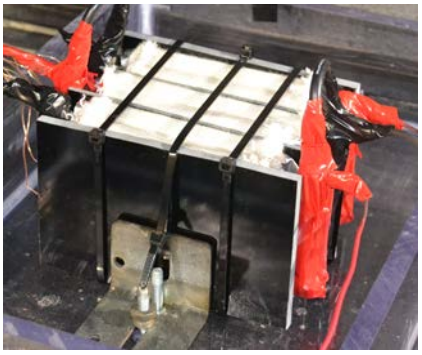

Figure 35. A 3 module stack (3S4P pack) before overcharge voltage was applied to center module (1S4P cell block)

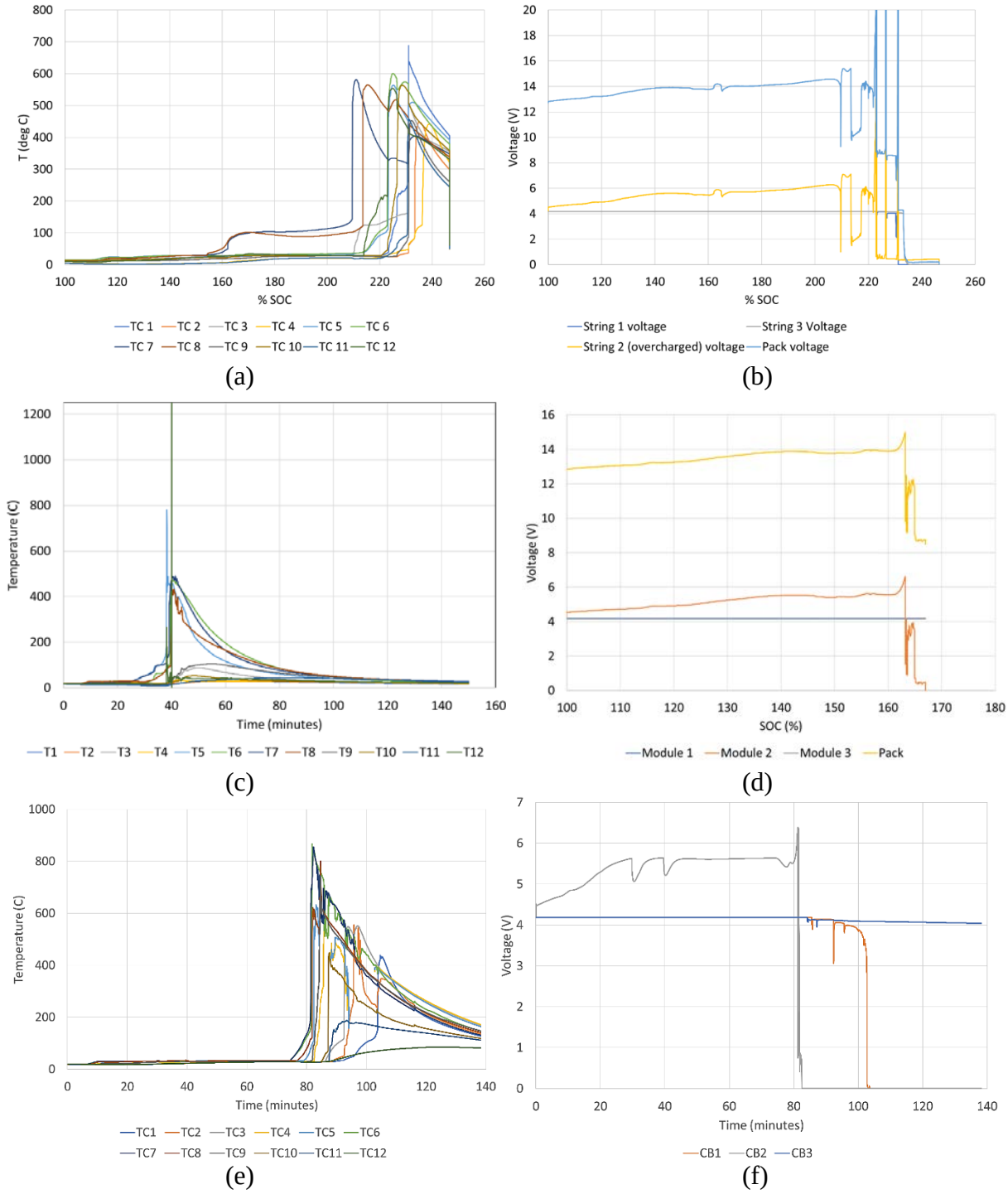

Figure 36. Results for central module (1S4P cell block) overcharge testing of a three-module stack (3S4P cell block) for different cell pack configurations: (a and b) temperature and voltage data for dual-stack configuration, shown in figure 9a (three modules touching each other); (c and d) temperature and voltage data for dual stack configuration shown in figure 9b (additional insulation layer in between modules); and (e and f) temperature and voltage data for single-stack configuration shown in figure 9c

Figure 37 shows the badly damaged remains of the single stack three-module test (corresponding to figure 9c) after the overcharge test. The broad conclusion at this stage: if the entire module (1S4P) fails, it propagates through the rest of the module, even with the packaging technology, unless there is physical separation or insulation in between the modules. That is, the cell packaging technology alone can handle a failure event triggered by the energy content from a 5 Ah cell failure and prevent propagation (e.g., single-cell failure triggered by nail penetration shown in figure 34), but it cannot fully prevent propagation of the energy released from a 20 Ah failure (four cells in parallel) without additional insulation.

Figure 37. The badly damaged remains of the single stack three-module (3S4P pack) after overcharge test of one of the three modules

It is important to note that the DO-311A requirements do not need prevention of propagation, triggered by an entire module failure (e.g. the 1S4P block of 20 Ah capacity in this test). Rather it calls for prevention of failure propagation in case of a single cell failure within the module, very similar to the nail penetration test condition show in figure 34. Based on the nail-penetration test results, it was felt that the packaging technology would enable prevention of failure propagation for the DO-311A test conditions. For the sake of completeness, a test of overcharging a single cell of the middle of the three-module stack was conducted in a sealed battery enclosure. Each cell in the three-module 3S4P pack was equipped with a 2-mm-thick packaging material. A 1C (5 A) charge was applied to cell 7 of the configuration shown in figure 9a. The overcharged cell began to slowly heat up and eventually reached thermal runaway after 95 minutes. The cell temperature rapidly peaked to 273°C, and the outgassing cell raised the box internal pressure to 100 psi where the pressure release valve was activated. The majority of the surrounding cells stayed in the 50°C range during the failure. Cell 6 was the only exception because it briefly reached 153°C but did not enter thermal runaway following the failure of its neighboring cell. The packaging technology with 2-mm-thick material proved to be capable of preventing failure propagation inside a sealed battery. Figure 38 shows the temperature and pressure data for the single cell overcharge test in a multi-module configuration.

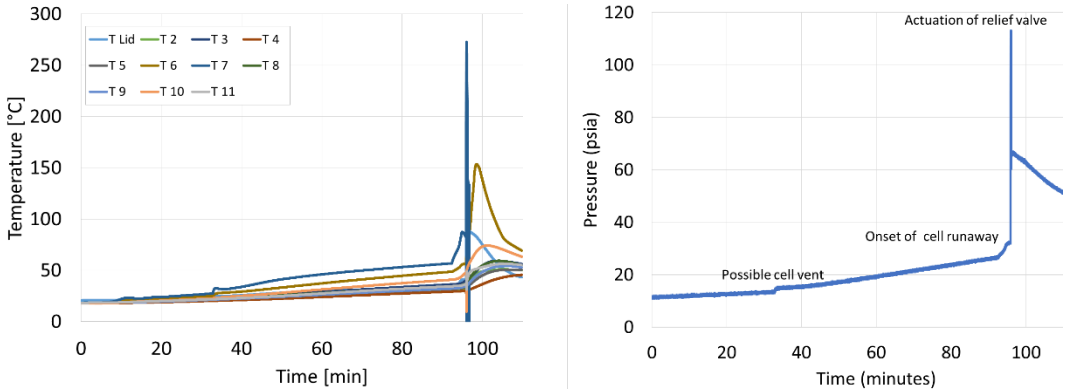

Figure 38. Results for a single-cell overcharge test on a three-module array (3S4P) in a sealed enclosure with pressure release valve: (a) cell temperatures, (b) enclosure pressure

4.4 BATTERY-LEVEL SAFETY CHARACTERIZATION

After investigating the effectiveness of the packaging technology at the module and multi-module level, a full-scale battery was tested. The two 26 V, 20 Ah battery test units spoken of in section 3.5 were prepared for battery-level failure testing. In the previous sub-section of multi-module-level safety characterization (section 4.3), nail-penetration and electrical-overcharge test results were shown of a single-cell failure (figures 34 and 38). For the battery-level testing, the test protocol laid out in Appendix C of DO-311A was followed, which calls for overcharging of electronically isolated, neighboring cell pairs in different locations around the cell pack of the full battery. Figure 39 shows a schematic diagram of the cell pack of the full battery (7S4P) and the chosen cell pair locations for overcharging. The two overcharged cell pairs were chosen to test the worst-case failure propagation scenarios. Being in the upper stack, the cell pairs (both 1 and 2) have slightly reduced cooling. Cell pair 1 is in contact with only three neighboring cells, resulting in possible energy build up in the failed cells. Cell pair 2 is in direct contact with six neighboring cells, increasing the chance of propagation. To electronically isolate and allow overcharging of the cell pairs, the internal wiring was modified and additional external terminals were installed to the enclosure. Neither test battery was equipped with a BMS, but the included BMS feedthrough was used for cell temperature and cell pack voltage collection during testing.

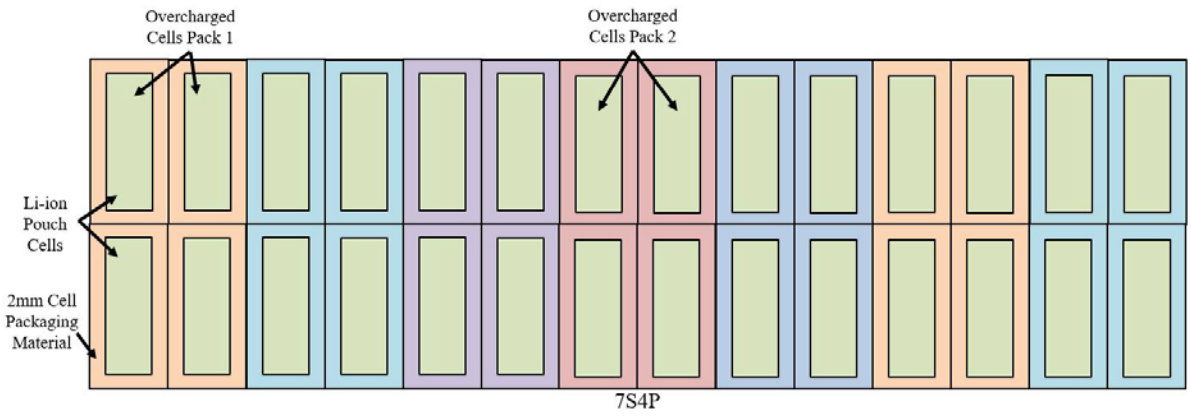

Figure 39. 7S4P cell pack arrangement showing the electronically isolated, neighboring cell pairs that will be overcharged during battery-level safety testing

Cell pack 1 was tested first, with the battery enclosure pressure release valve set to 50 psi. The overcharge test started with the pack at 100% SOC, or fully charged. A 1C, 5 amp charge was applied to the electronically isolated, neighboring cell pair. The pair of cells went into thermal runaway after 83 minutes of overcharge or at an SOC of 239%. The temperature quickly reached over 250°C. At this point the internal pressure of the battery box rapidly increased. Unfortunately, at this point the lid attachment mechanically failed, and the lid was rapidly pushed off, as shown in figure 40. All voltage and cell temperature data were lost because the communication wires were torn free from the feedthrough that was bolted to the lid. With communication to the battery lost, the battery was allowed to continue venting and cooling overnight, whereupon it could be visually inspected. Through visual inspection, it was determined that the overcharged cells had indeed fully ruptured and failed, but failure propagation did not occur. Despite the prevention of failure propagation, these results would fail the acceptance criteria of DO-311A Appendix C, which specifies that failure propagation is acceptable, but all battery failure emissions must escape only through the designed venting provisions. With the failure of the battery box lid, the cell effluence was vented directly to atmosphere through the open top.

Figure 40. Overcharged edge cell pair caused the battery box lid to be blown off, resulting in cell effluence rapidly venting to ambient

On cell pack 2, the lid-attachment method was modified to increase the pressure-containment strength. The pressure-release valve setting was reduced to 25 psi. The overcharge test again started with the pack at 100% SOC. The overcharge current was applied to the center electronically isolated, neighboring cell pair. The pair of cells went into thermal runaway after 80 minutes of overcharge or at an SOC of 233%. The temperature rapidly increased and the integrated pressure release valve activated and released the initial cell effluents. The spring-loaded relief valve then resealed. After the initial cell failure, the battery continued to be monitored. Over the next 30 minutes the failure slowly progressed through the rest of the battery pack, causing periodic subsequent actuations of the pressure release valve. The slow progress of the failure and repeated release valve actuations were monitored through a video recording of the test. The battery box remained sealed throughout the entire process with venting occurring only at the integrated pressure release valve. This result would successfully fulfill the requirements of the DO-311A Appendix C. Because of the failure propagation throughout the battery, the internal wiring was compromised resulting in unusable internal temperature data, but thermocouples placed on the exterior of the enclosure survived unscathed (figure 41).

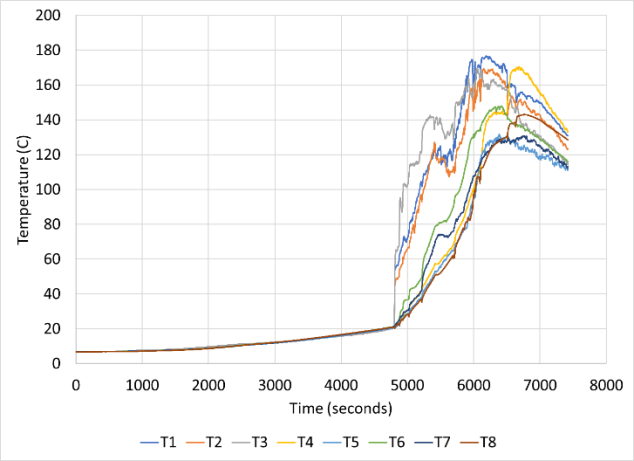

Figure 41. External battery box temperatures during overcharge failure testing of the center cell pair

Figure 41 shows the thermocouple results from the external enclosure wall, where the exterior of the battery box reached ~180°C in some areas. It was a gradual rise as the failure slowly progressed through the entire battery. Based on the external temperature data and the video, it is believed that hot effluents were not fully released out of the enclosure after each failure. Effluents were released intermittently as long the internal chamber pressure exceeded the set pressure of the release valve. After each pack failure, there was a brief cooling of the external wall, until the next failure. It is believed that the presence of residual hot effluent within the enclosure was the reason the packaging technology failed to prevent the failure propagation. In the first test, the lid failure allowed the hot cell effluents to quickly vent from the enclosure allowing the packing technology to isolate the failure to the overcharged cell pair. In the second test, part of the effluents was released in a controlled fashion, but the remaining portion added to thermal buildup.

The current hypothesis, based on the two battery-level failure propagation experiments, is as follows. Two mechanisms contribute to the failure propagation in an enclosed battery system: (1) cell-to-cell heat dump by direct contact between cells and modules and (2) impingement of hot effluents on neighboring cells, generating another method of heat dump. In the first experiment, the second mechanism did not come to play as the effluents were released by the lid failure. The cell packaging technology handled the first mechanism very well. As long as there is a method to quickly remove the ejecta from the enclosure, the second mechanism can be avoided. It is believed that in the second experiment, the intermittent pressure relief was not enough to prevent internal temperature buildup.

Future work needs to focus on the vent design to increase cross sectional area to allow rapid vent out. In addition, implementation of a burst disk into the vent design would be beneficial to ensure that once a failure has occurred and pressure has been released, the system is permanently open to the outside environment (outside the enclosure) rather than intermittently open as with a spring-driven pressure-release valve.

5. CONCLUSION

With this report, Teledyne concludes a 22-month effort on investigating the effectiveness of a multi-functional packaging technology to prevent cell-to-cell failure propagation in a Lithium-ion battery, thus averting catastrophic failure. The concept of the passive packaging technology is based on placement of a material around the individual cells of a Li-ion battery. The technology has the ability to act as a thermal management system both under normal operation and in the case of a local cell failure. As a demonstration platform, 26 V, 20 Ah batteries were developed, prototyped, and tested, which in the future could be used as a helicopter starter battery, a drop-in Li-ion version of the current 7246-20 24 V, 20 Ah Valve regulated lead acid (VRLA) helicopter starter battery. The demonstrator batteries were built with cells of highly volatile and energetic lithium cobalt oxide chemistry.

These lithium batteries were subjected to mechanical, thermal, and electrical abuse conditions. The abuse tests were carried out first at the single cell-level (3.7 V, 5 Ah), then at module-level (3.7 V, 20 Ah in 1S4P configuration), then at multi-module-level (11.1 V, 20 Ah in 3S4P configuration), and finally at full battery level (25.9 V, 20 Ah in 7S4P configuration). The packaging technology is designed to prevent cell-to-cell failure propagation and not a local cell failure. Therefore, technology was not employed on the single cell-level tests. At the module-level, it was demonstrated that failure of a single cell in the module does not propagate through the rest of the module with the packaging technology. At the multi module-level, it was demonstrated that even the failure of an entire module (a 1S4P block of 20 Ah capacity) can be contained and prevented from propagating to the neighboring modules. At the full battery level, failure propagation tests were carried out with single and multiple cell failure (two trigger cells) at the worst failure configurations. The results show no cell-to-cell failure propagation as long as the effluents of the failed cells are vented out, preventing heat propagation through the ejecta. The full battery-level tests underscored the importance of venting, in addition to the thermal dump to the neighboring cells.

As part of the demonstrator battery build up, functional tests were also carried out on the 26 V, 20 Ah batteries, characterizing their instantaneous current rating (756 amps for 0.3 s, commonly

termed as I_{pp} in avionics starter batteries and 403 amps for 15 s, commonly termed as I_{pr}) and driving them under helicopter starter load profiles. The cell case temperature rise was < 10°C for all test cases in spite of the high in-rush current, which allows the battery to perform multiple aircraft engine starts without risk of thermal degradation and reduced cycle life.

After a successful closure of the program, opportunities are being explored to mature the technology further, raise its manufacturing readiness level, and transition to the avionics market. As part of the technology maturation process, future efforts need to focus on: (1) further investigation of the battery vent design to improve the likelihood of prevention failure propagation for multi-cell failures inside a tightly conforming enclosure; (2) simplifying and streamlining the packaging technology to increase manufacturability and adaptability to different cell designs; (3) establishing long-term reliability and ruggedization for airborne applications; and (4) FAA qualification testing including DO-311A tests.

6. IMPACT OF THE PROGRAM TO THE AVIATION COMMUNITY

Safety has been a key concern of widespread adoption and deployment of Li-ion batteries in avionics platforms. The packaging technology investigated in this program provides a path for mitigating some of these concerns. As the technology further matures, it can be extended to other cells, enabling the use of energy/power-dense cells with volatile chemistries in airborne applications, which would otherwise be dismissed because of safety concerns. With further experimentation of this technology and proving its efficacy on a repeatable and reliable basis under stringent design specifications, this solution may reduce some of the preliminary safety-testing procedures normally performed when qualifying a new li-ion battery design. The utility of the technology in preventing cell-to-cell failure propagation was proven in a step-by-step process, with the worst-case scenario considerations. The procedure may be adopted for qualification of Li-ion batteries.

APPENDIX A—TELEDYNE SCIENTIFIC COMPANY PROPRIETARY DATA

This information is available upon request.